161

SATELLITE & MESOMETEOROLOGY
RESEARCH PROJECT

Department of the Geophysical Sciences
The University of Chicago

DOWNBURSTS AND TORNADOES OF 6 AUGUST 1977 NEAR SPRINGFIELD, ILLINOIS

T. Theodore Fujita

SMRP Research Paper 161
November 1978

DOWNBURSTS AND TORNADOES OF 6 AUGUST 1977 NEAR SPRINGFIELD, ILLINOIS

Gregory S. Forbes

and

Roger M. Wakimoto

SMRP Research Paper No. 161

November 1978

TABLE OF CONTENTS

Downbursts and Tornadoes of 6 August 1977
Near Springfield, Illinois

Gregory S. Forbes
and
Roger M. Wakimoto

ABSTRACT

This paper presents results from a case study of a remarkable windstorm. Aerial and ground surveys revealed that 17 cyclonic tornadoes, 1 anticyclonic tornado, 10 downbursts, and 19 microbursts occurred from a thunderstorm complex in a rather limited region of Central Illinois. Examples of the patterns of damage associated with each of these phenomena are presented.

These examples not only include typical damage, but also include evidence of substructure within each of the phenomena. Examples of interactions between downbursts, microbursts, and tornadoes are also presented. In addition, the meteorological conditions accompanying and perhaps identifying the downburst storm are presented on radar and satellite imagery, and on the synoptic scale.

Downbursts and Tornadoes of 6 August 1977
Near Springfield, Illinois

Gregory S. Forbes
and
Roger M. Wakimoto

> It got really still and I saw the sky turn green to the north. Then it started to rain and the wind picked up suddenly. I watched the doghouse blow away and saw the puppies flying through the air. It was raining so hard that you could barely see, and trees were bending over to within six feet of touching the ground. The warranty says my TV antenna was built to withstand 100 mph winds, and it was bent and twisted. The noise sounded like a locomotive roar, and it must have been a tornado, but I never saw a funnel.[1]

1. INTRODUCTION

At one time or another, even persons with no interest in the weather have experienced the strong, gusty surface winds which often accompany thunderstorms. Fortunately, however, few have had to endure the type of windstorm described above by S. J. Brunk. This report documents and analyzes this storm which, directly or indirectly, affected literally thousands of persons in Sangamon County and the nearby counties of central Illinois on August 6, 1977, between the hours of 1600 and 1730 CDT (2100 - 2230 GMT).

With this windstorm also came tornadoes and torrential rains, whose combined effects caused extensive property damage, numerous power disruptions, and flash flooding. The swath of wind damage was over 66 miles (106 km) long, averaged about 5 - 6 miles in width, and affected portions of at least 5 counties. In some regions the swath was 8 miles (13 km) wide.

---

[1] Eyewitness account of S. J. Brunk, Jr., who experienced the effects of downburst 9, about 0.9 mi (1.5 km) west of Beamington.

Figure 1 illustrates the damage pattern of the Springfield storm. In all, there were 10 downbursts,[2] 19 microbursts, and 18 tornadoes. In fact, portions of the damage swath, including two downbursts, were not included in Figure 1. Surveyed damage extended about 9 miles (14 km) west and 18 miles (29 km) east of the boundaries of Map 1. There were further reports of crop damage near Murrayville (several additional miles southwest) which were not investigated.

Documentation of the extensive damage required a major survey effort. The authors performed aerial surveys on four days (August 12, 20, 22 and 27), with a total of about 30 hours of survey time. Roughly, 1600 photos were taken of the damage. In order to unscramble the sequence of weather events, the authors subsequently performed a 3-day ground survey (September 3 - 5), interviewing about 86 residents.

In addition to revealing the overall damage patterns of Figure 1, the surveys also revealed many complex damage patterns. Figure 2 illustrates one of the most complex regions of damage, with stray suction vortices (b, c, d) of the South Fork tornado (7)[3] occurring between microbursts m 5 and m 6. It will later be shown (Section 5.6) that each of these vortices possessed a "spin-up mark," revealing the concentration of downburst-related vorticity to produce the incipient vortex.

Additional details of the characteristics of downbursts, microbursts, and tornadoes and their relationships are given in later sections. Radar, satellite, and surface and upper-air observations are analyzed to understand the formation and detection of downburst-producing thunderstorms.

---

[2]The term "downburst" was introduced by Fujita (1976) to explain the extreme and localized downdraft which caused the crash of a commercial airliner. When the downburst approaches the ground, vigorous lateral spreading of the downburst results in damaging horizontal winds. Within the relatively large downburst, there are often highly-localized diffluent patterns of damage, referred to as "microbursts". Fujita (1978) has compiled and analyzed numerous cases of storms containing downbursts and microbursts.

[3]Numbers in parentheses following a tornado name refer to the tornado number on Figure 1.

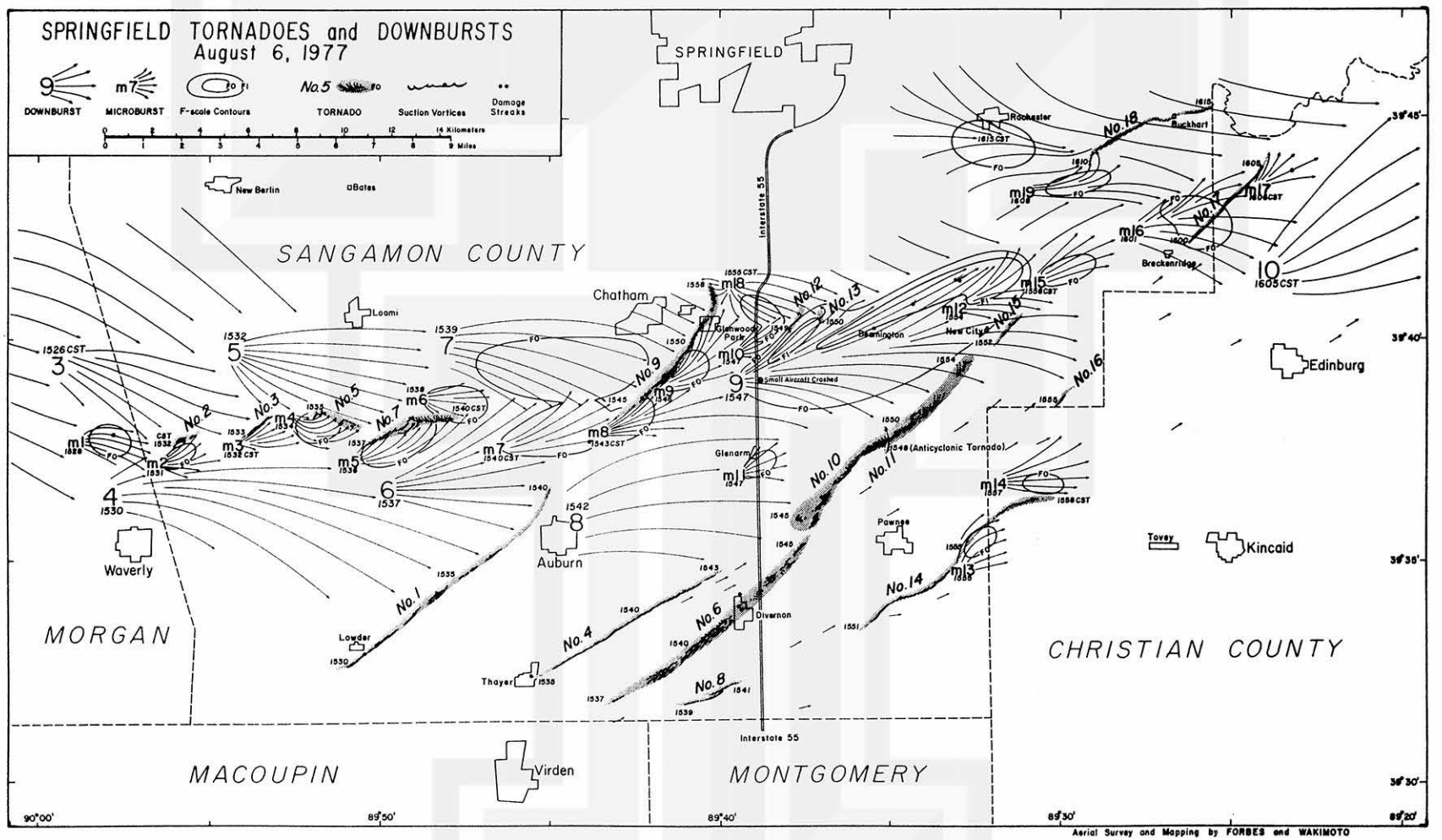

Figure 1. The Springfield storm.

Figure 2. Stray vortices in the South Fork tornado, flanked by microbursts m 5 and m 6.

2. PRECURSORS TO THE DOWNBURST

The Springfield windstorm was not associated with an extensive, rapidly-moving squall line. Instead, the windstorm was associated with a rather small echo configuration, a bow echo (Fujita, 1978). The bow echo occurred just south of a slowly-moving, nearly-stationary cold front. In fact, showers and thundershowers had occurred in the same area during the previous night. Because the synoptic-scale triggers were so subtle, the evolution of the Springfield storm is given a closer examination in this chapter.

2.1 The Synoptic Scale

Figure 3, the 500-mb analysis for 1200 GMT on August 6, shows that the downburst area was located within the long wave ridge. Accordingly, 500-mb temperatures over Illinois were exceptionally warm. Surface temperatures and dewpoints were also high.

A short wave trough can be seen entering the ridge. The upward motion in advance of the trough was one of the key factors favoring thunderstorm development.

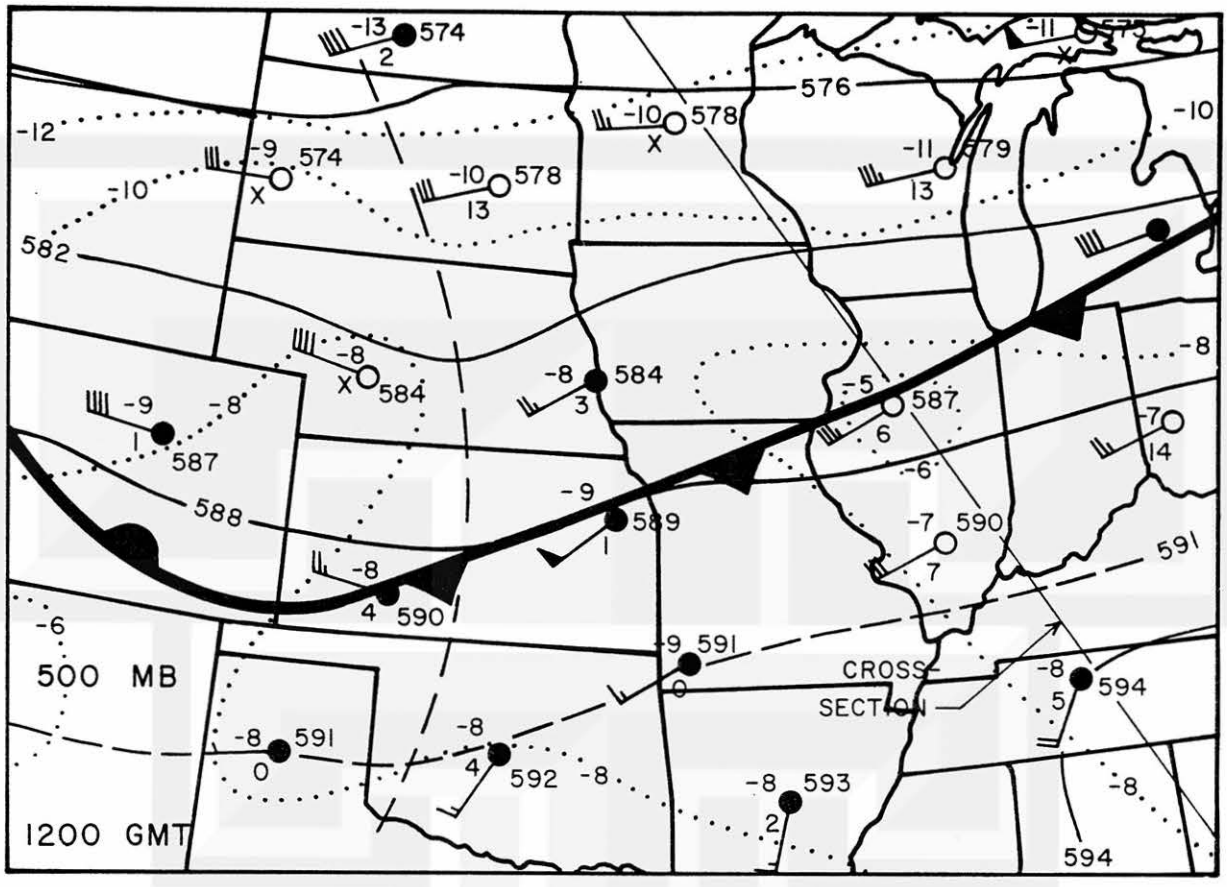

Figure 3. 500 mb analysis, 1200 GMT, 6 August 1977.

Superimposed on the 500-mb analysis is the position of the surface cold front. Since the upper flow nearly parallels the front, its slow movement is understandable. Also shown on the 500-mb analysis is the location of NW - SE cross-sections used to evaluate the vertical structure of the thermal and wind fields.

Figures 4 and 5 are subjectively-analyzed adiabatic cross-sections for 1200 GMT August 6 and 0000 GMT August 7, respectively. The pronounced stable layer near the surface at 1200 GMT was apparently transformed to a nearly-adiabatic layer at 0000 GMT by insolation. The cross-sections do not readily delineate the indicated positions of the weak fronts analyzed on the surface map. Northwest of SLO, however, the slope of the adiabats throughout the entire troposphere is dramatic, indicating a deep baroclinic layer.

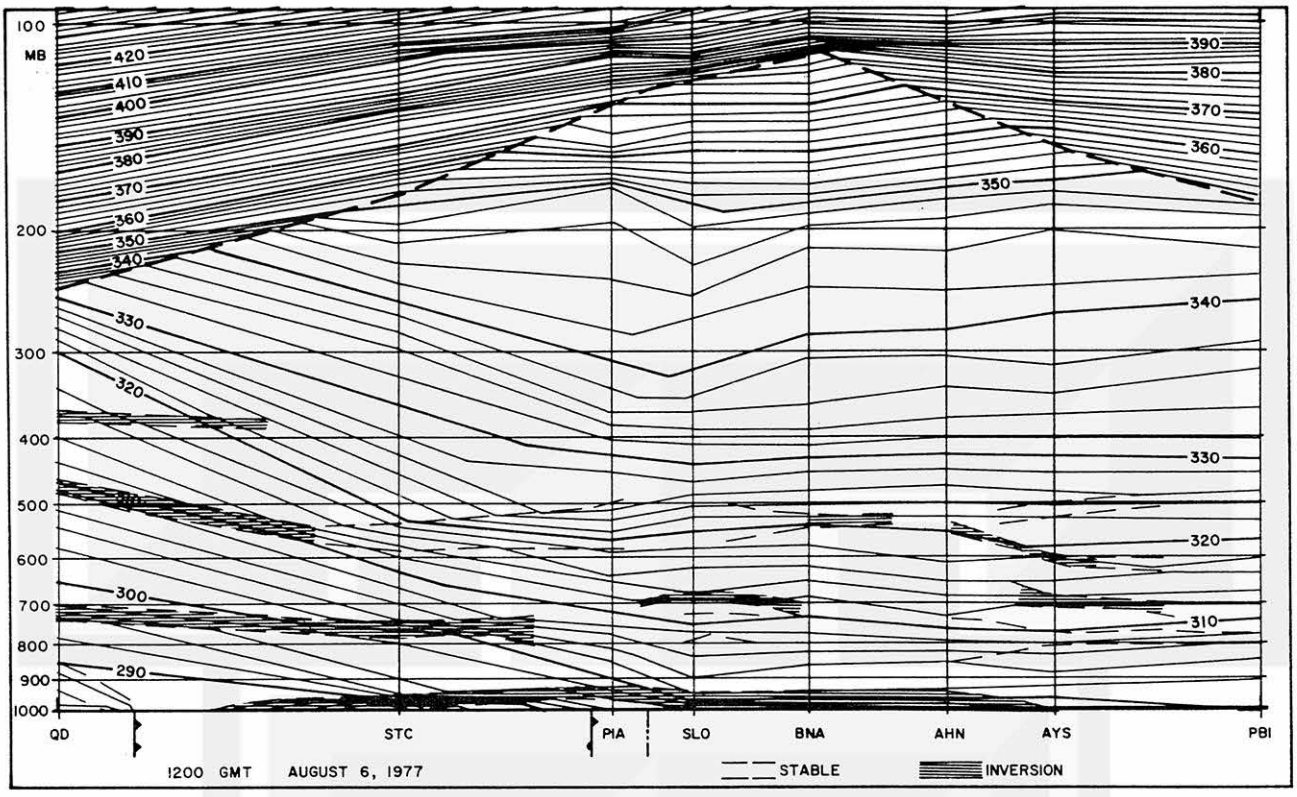

Figure 4. Adiabatic cross section, 1200 GMT, 6 August 1977.

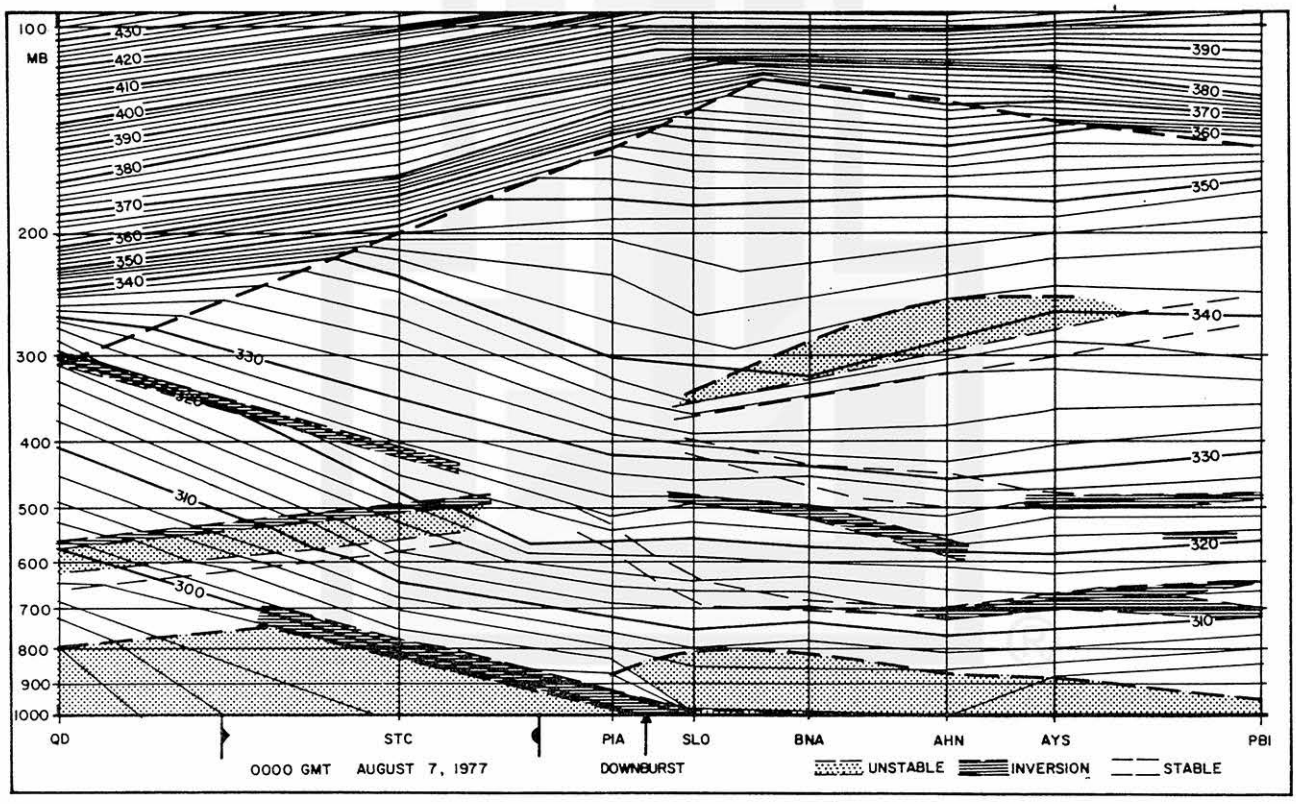

Figure 5. Adiabatic cross section, 0000 GMT, 7 August 1977.

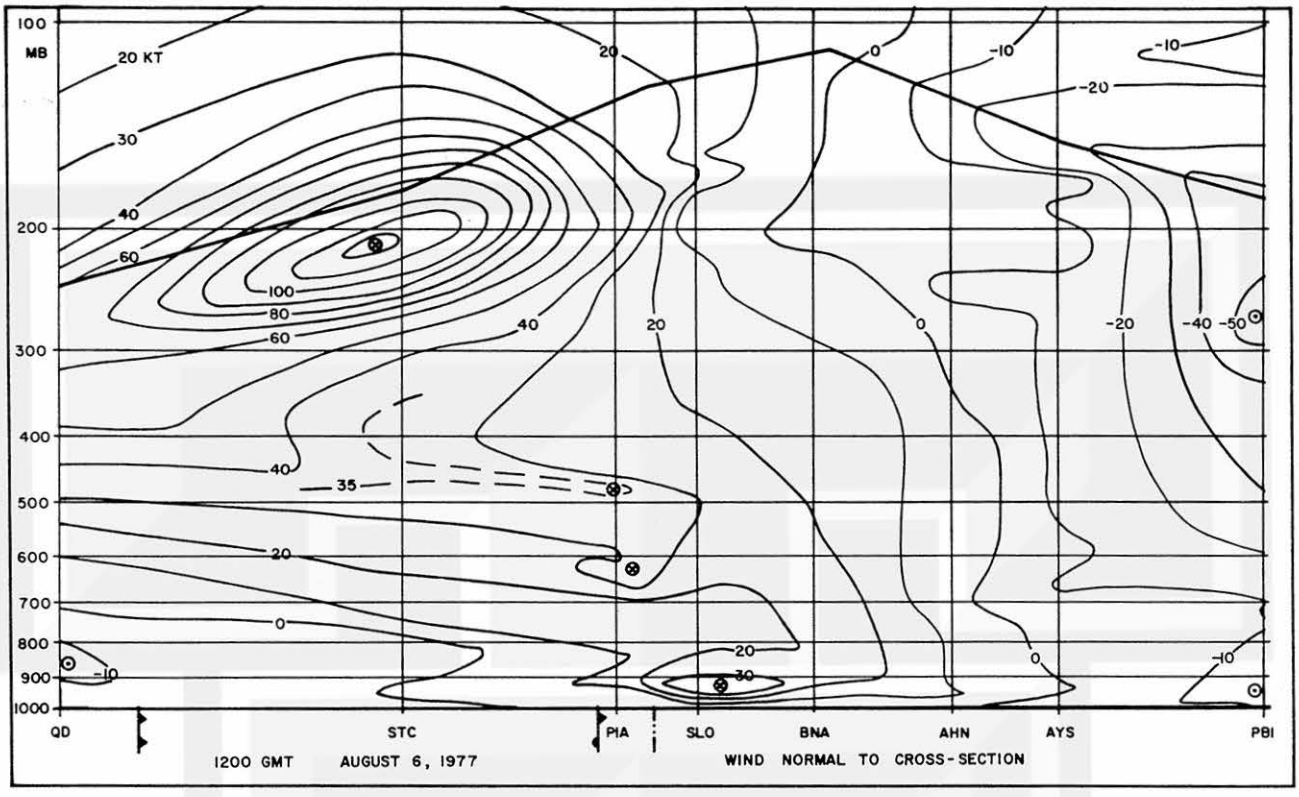

Figure 6. Component of the winds normal to the cross-section of Figure 35, 1200 GMT, 6 August 1977.

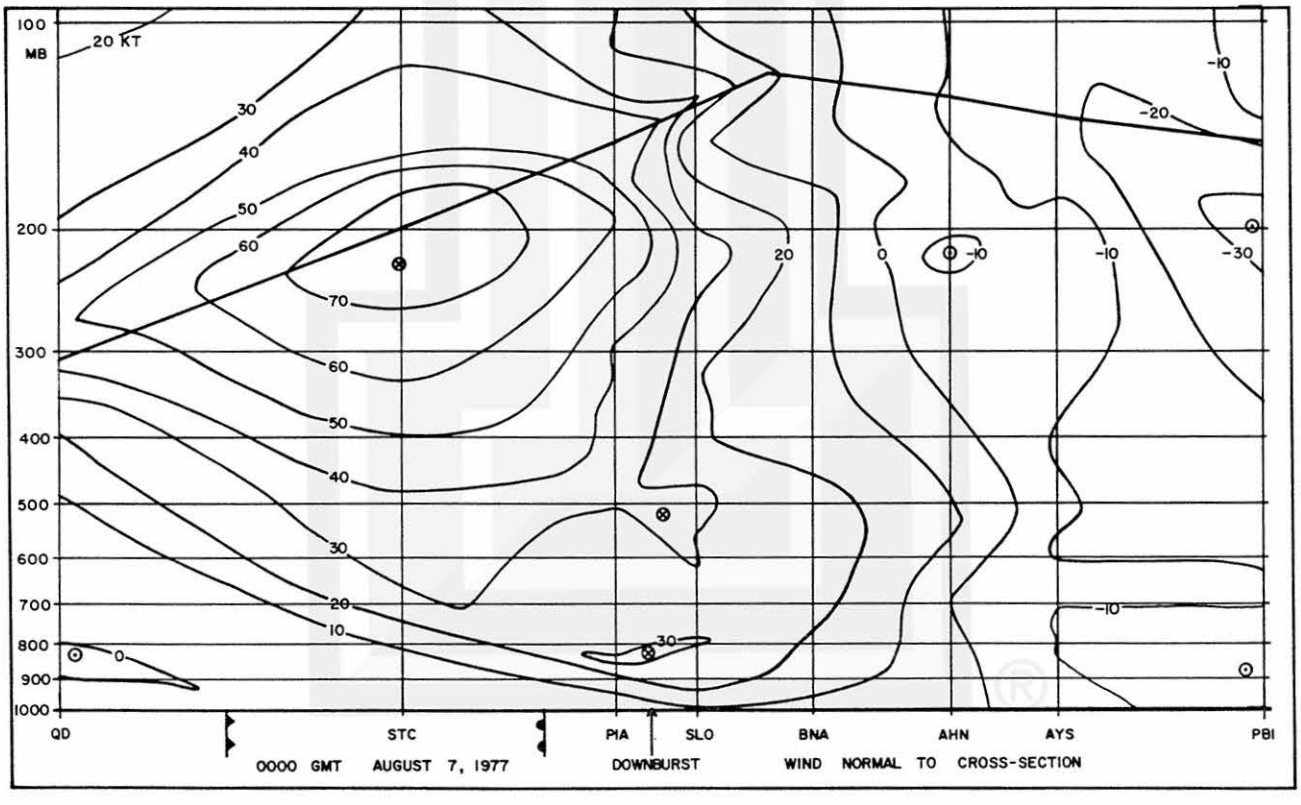

Figure 7. Component of the winds normal to the cross-section of Figure 36, 0000 GMT, 7 August 1977.

Figures 6 and 7 present the component of windspeed normal to the cross-sections at 1200 GMT August 6 and 0000 GMT August 7. The axis of the southwesterly jet crosses the section near STC. The core of strongest winds within the jet moved to the northeast by 0000 GMT, resulting in windspeeds decreasing over STC between 1200 and 0000 GMT.

Between 1200 and 0000 GMT, however, the jet axis appeared to shift to the southeast and descend, resulting in increased winds over PIA. In addition, the low-level jet became positioned near PIA at about 830 mb by 0000 GMT. It is likely that these windspeed increases contributed to the possibility of the downburst.

Figure 8 shows the component of the winds along the cross-section at 1200 GMT. Southeastward velocities near STC are consistent with a southeastward movement of the jet. Confluence is indicated near PIA and SLO near 750 and 200 mb. At the surface, there was a line of divergence near St. Louis (near SLO on the section), oriented approximately northeast-southwest, that may have been related to the upper confluence. This

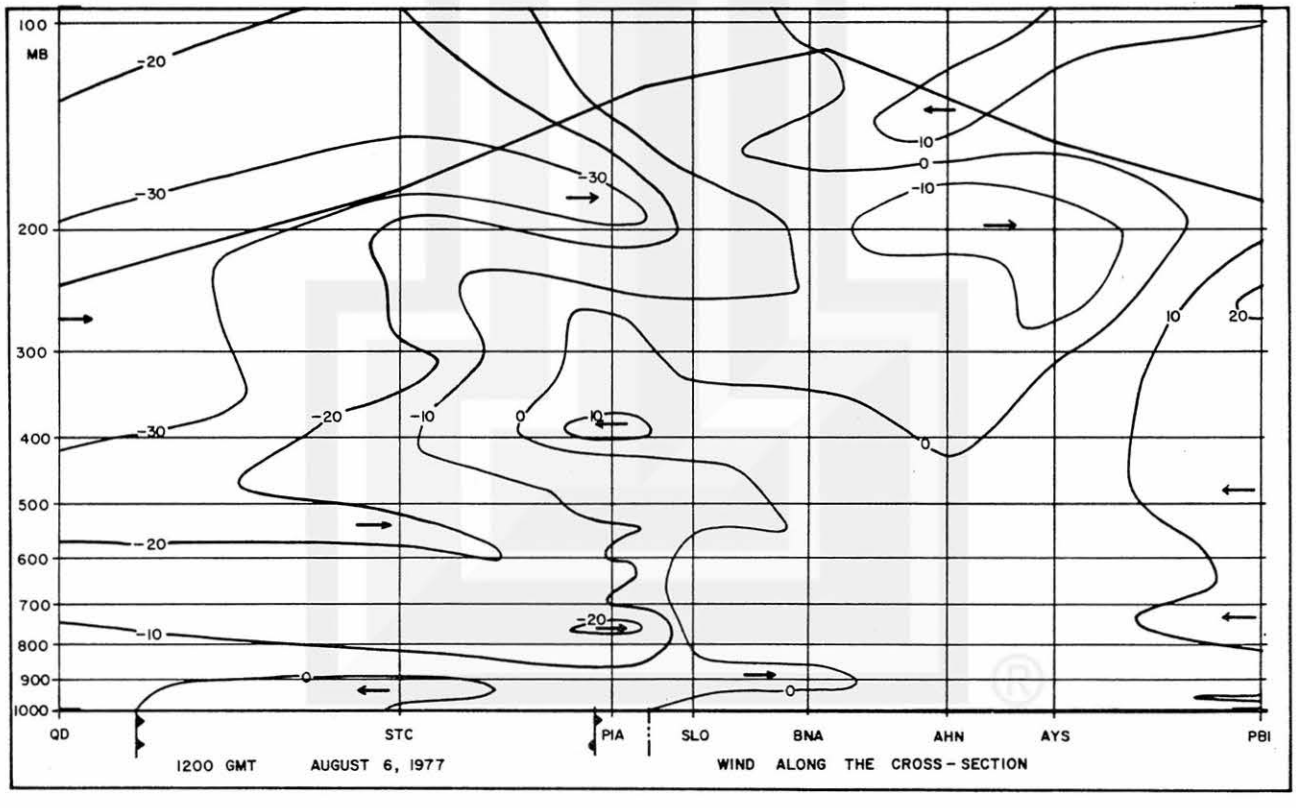

Figure 8. Component of the winds along the cross-section of Figure 35, 1200 GMT, 6 August 1977.

line of surface divergence marked the northwest edge of a region of scattered cumuli. Clear skies occurred to the northwest of the line. The line thus appeared to be a moisture boundary.

2.2 The Mesoscale

The Springfield area had been visited by thunderstorms on the night of August 5-6. Figure 9 presents the surface analysis for 1300 GMT. A line echo wave pattern (LEWP) on STL radar is superimposed. This wave pattern travelled east-northeastward along the cold front and finally dissipated in northern Illinois. This LEWP is also visible in the 1230 GMT visible satellite imagery, Figure 10.

Figure 11 presents the 1830 GMT visible satellite imagery. Superimposed on the figure are the positions of the cold front and moisture boundary mentioned earlier.

At 1830 the Springfield storm complex is developing in northeast Missouri. A patch of clearing is developing behind the complex--an interesting sidelight to be discussed later. Also visible at 1830 are the remnants of the previous night's storms, now located in east-central Illinois and northwest Indiana.

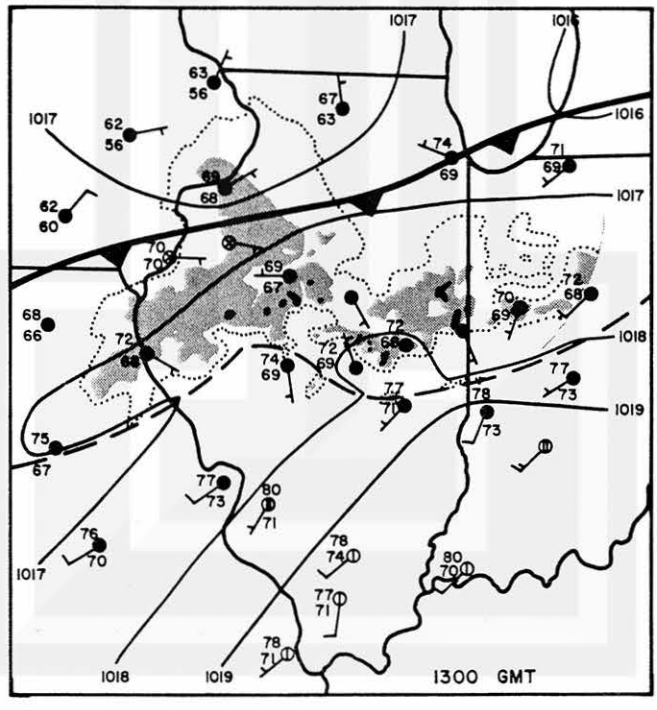

Figure 9. Surface analysis, 1300 GMT, 6 August 1977.

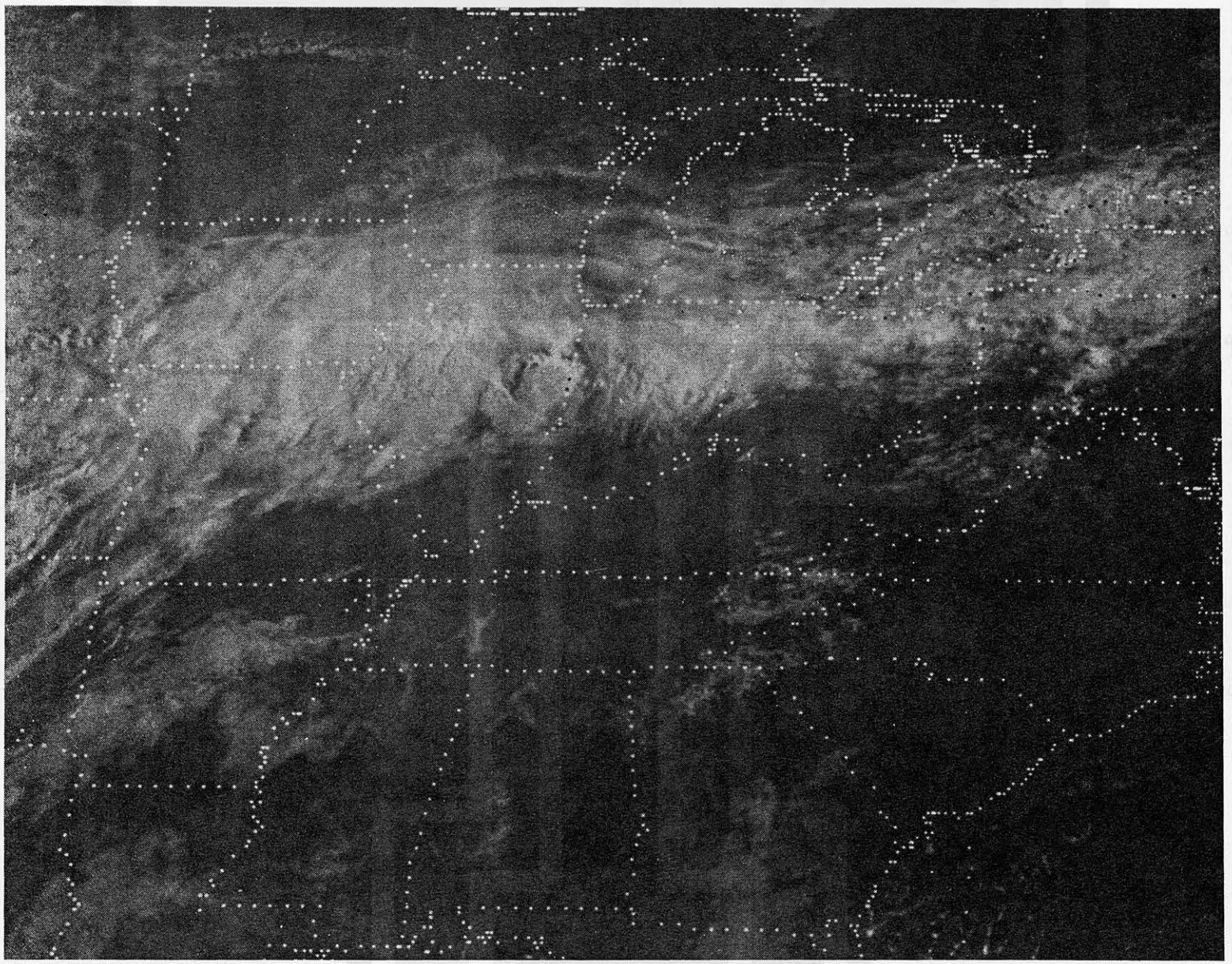

Figure 10. SMS visible satellite imagery, 1230 GMT, 6 August 1977.

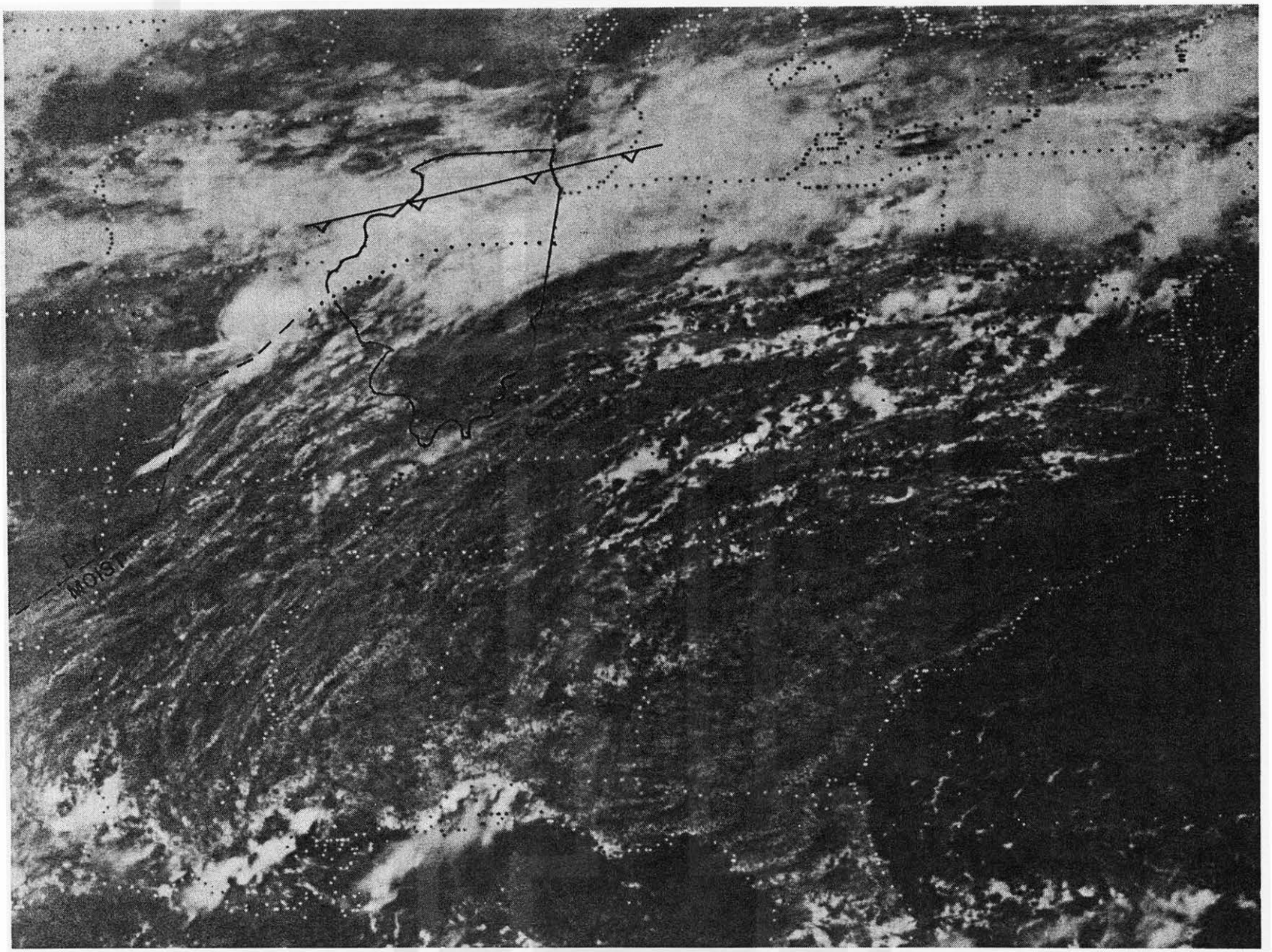

Figure 11. SMS visible satellite imagery, 1830 GMT, 6 August 1977.

The Springfield storm formed in the vicinity of three boundaries. Two were mentioned in Section 2.1. (1) It formed south of the W - E cold front, a substantial temperature and moisture boundary. (2) The storm grew explosively as it reached the NE - SW moisture boundary, where surface dewpoints then reached as high as 78 F (26 C). These boundaries are visible in Figure 11.

The third boundary is not readily apparent in Figure 11. It was the edge of a cold dome (mesohigh) produced by the previous night's storms in northern and central Illinois and western Indiana. Figure 12 shows the 1200 GMT Peoria sounding, taken with thunderstorms in the vicinity. The sounding is nearly moist adiabatic.

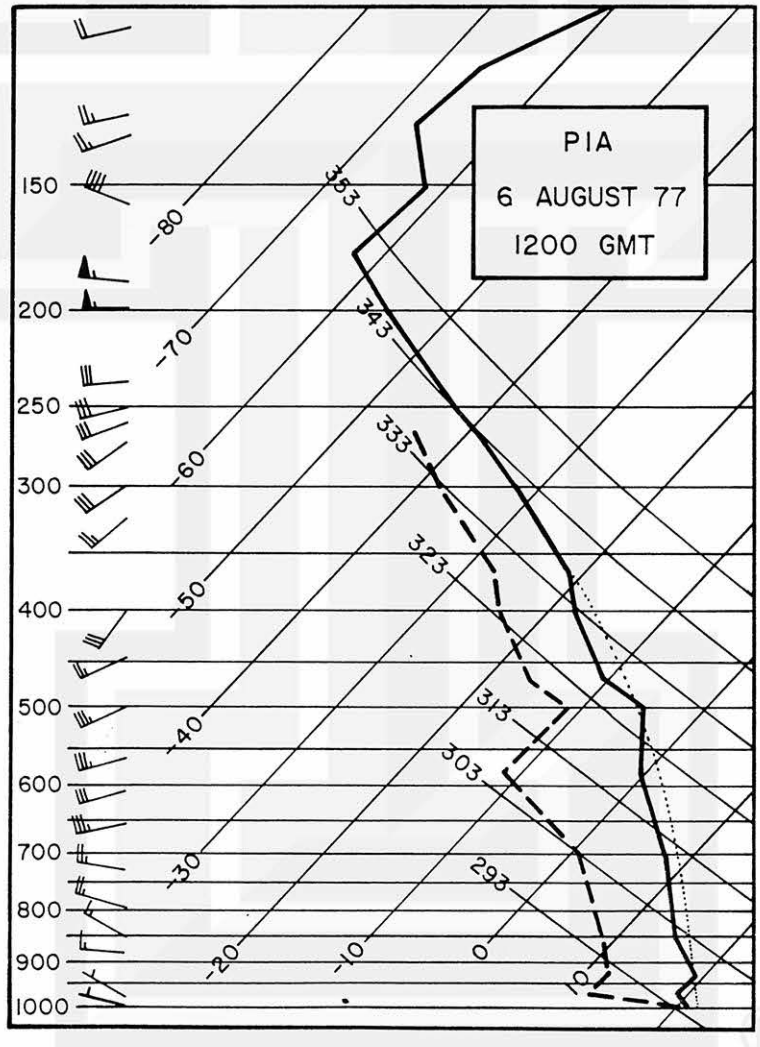

Figure 12. Sounding at Peoria, IL (PIA), 1200 GMT, 6 August 1977.

During the morning the western portion of this cold dome weakened, and its southern edge retreated northward, much like a mesoscale warm front. This boundary can be seen stretching east - west across Illinois at 1800 GMT, in Figure 13. Temperatures and dewpoints were considerably warmer south of this boundary.

There was possibly one additional factor in the development of the Springfield downbursts. A small line of echoes and an associated wind shift passed over the future route of the downbursts at 1800 GMT, shown in Figure 13. Surface winds retained their westerly component thereafter. If the wind shifts extended upward beyond the surface, this wind shift line may have set the corridor for the downburst. The mean wind in this corridor may have been altered by the wind shift, allowing the central part of a line of echoes to accelerate, becoming the Springfield bow echo.

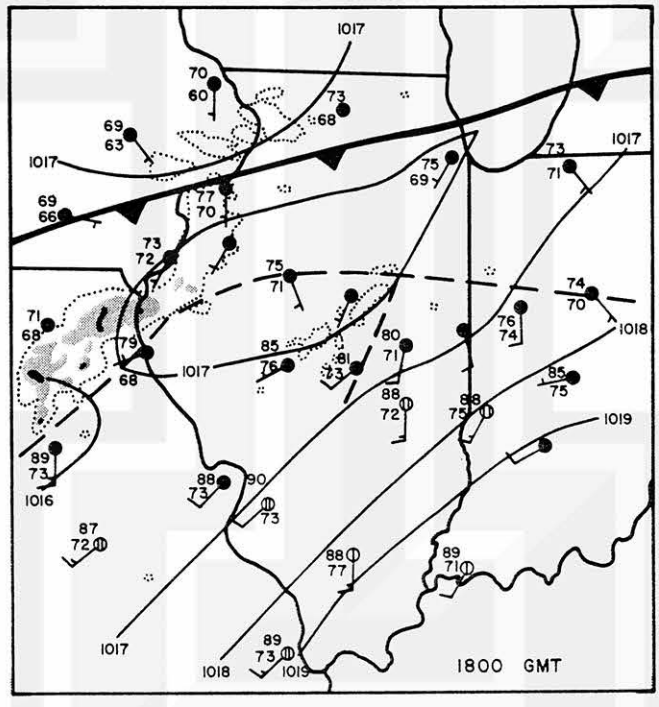

Figure 13. Surface analysis, 1800 GMT, 6 August 1977.

In summary, there were several significant synoptic and mesoscale features which probably contributed to the development of the Springfield storm:

1. A short wave approached the area at 500 mb.
2. Strong upper winds descended to very low levels in the vicinity of the storm.
3. The storm developed in a neighborhood where three boundaries existed: a cold front, a moisture front and a mesoscale boundary left from the previous night's thunderstorms.
4. A wind shift line in advance of the storm turned the winds ahead of the bow echo in the direction of storm movement.

Synoptic analyses detected the several factors presented above that gave a favorable setting for the downburst occurrence. The synoptic network in this case failed to indicate the existence of such a damaging storm, however. Figure 14 presents the surface analysis at 2200 GMT, with downbursts in progress. Only typical wind shifts are observed in the vicinity of the thunderstorms. For detecting the downburst, we shall turn to radar and satellite, as presented in Section 3.

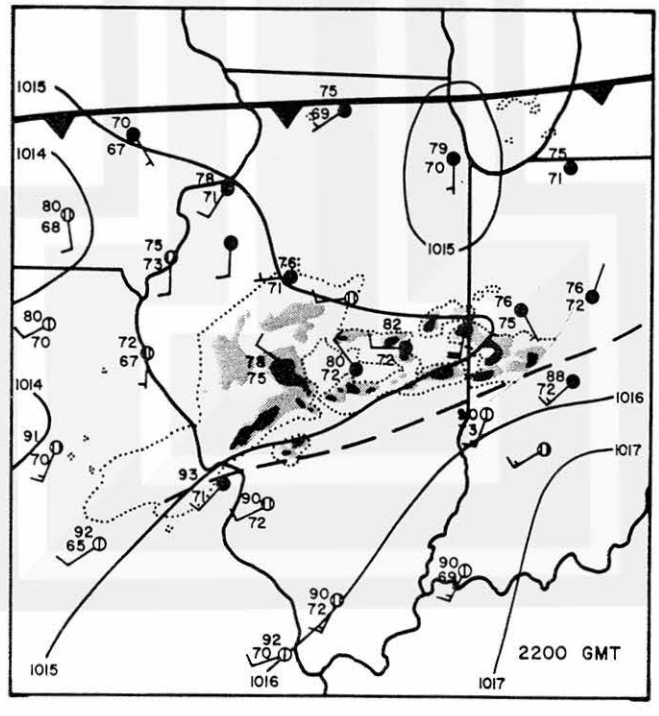

Figure 14. Surface analysis, 2200 GMT, 6 August 1977.

2.3 A Sidelight

An interesting mesoscale feature was visible in Figure 11, the clear area behind the Springfield storm. It is discussed here as a sidelight, as it did not appear to play a role in the development of the storm. Instead, it appeared to be an effect. The clear patch grew as the storm complex grew. The clear patch maintained the approximate shape of the storm complex.

Figure 15 shows the rainfall that occurred from the time of development of the storm (about 1500 GMT) until 2100 GMT. The visible satellite imagery at 2130 GMT is shown in Figure 16. Notice that the north - south widths of the clear patch and the

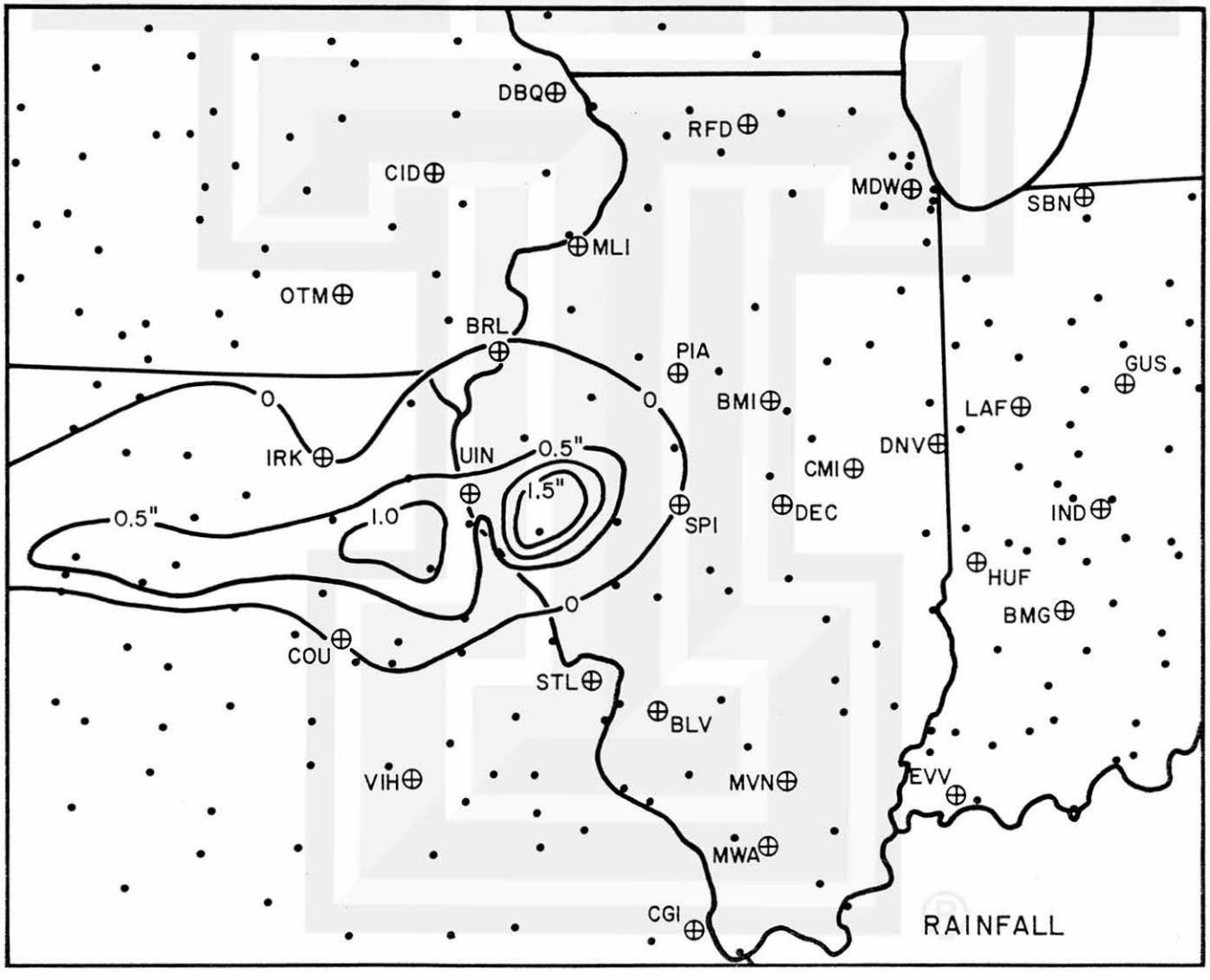

Figure 15. Rainfall between 1500 GMT and 2100 GMT, 6 August 1977.

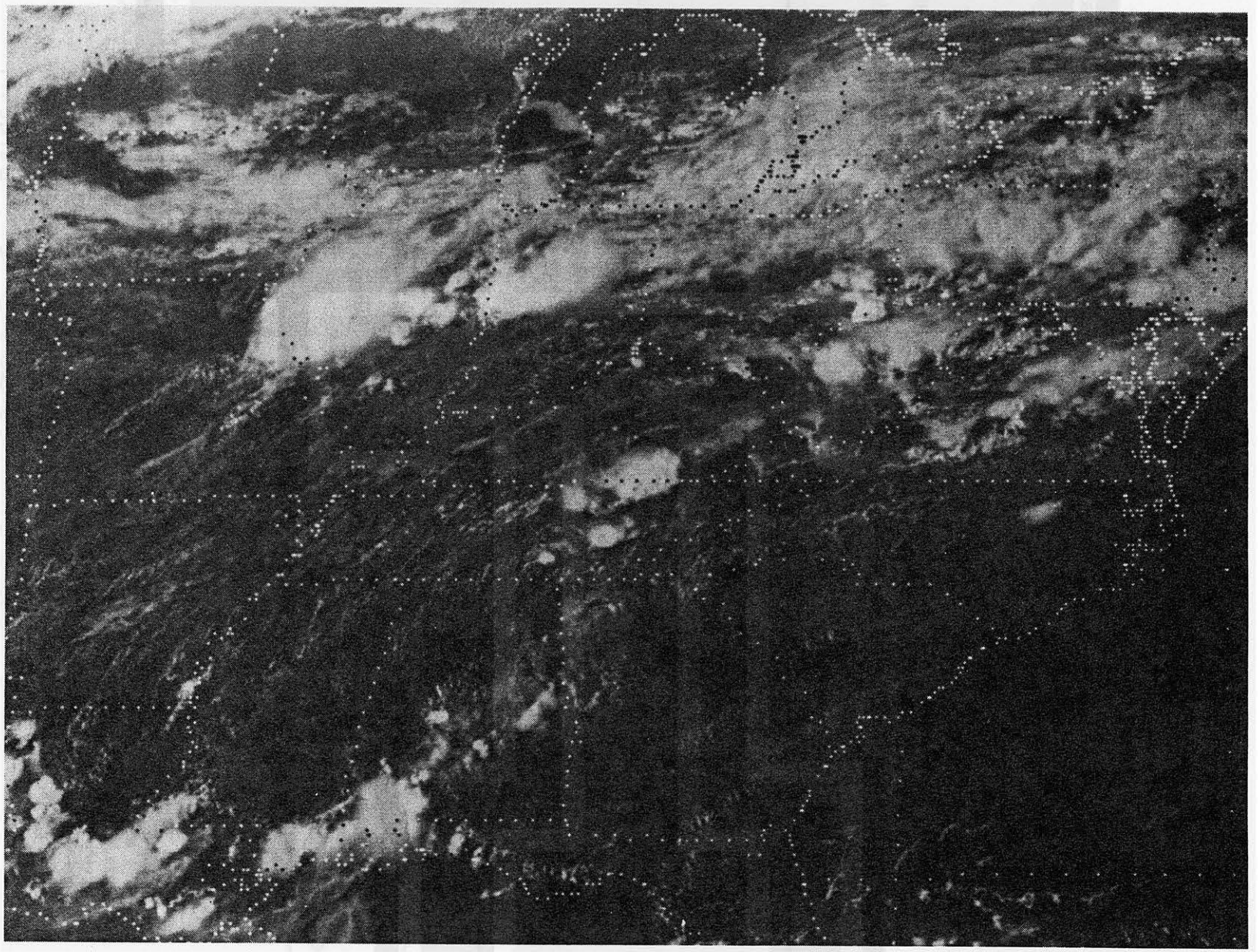

Figure 16. SMS visible satellite imagery, 2130 GMT, 6 August 1977.

rainfall swaths are very similar. Furthermore, there is a correlation between the rain-free area near IRK and the cloud intrusion from the north. Also, it should be noted that the western boundary of the clear patch was moving at the same speed as the complex. This suggests that clouds developed a certain time interval after the storm had passed.

Normally, this clear region might be attributed to a mesohigh. Because the air was initially cool and almost saturated from the previous night's thunderstorm activity, however, rapid evaporative cooling probably did not take place within the Springfield storm. Instead, evaporation occurred only slowly and mesohigh development was minimal. It is likely that cloud development was suppressed by the fact that post-storm insolation could not raise temperatures without also evaporating surface water, and, hence, instability did not develop for several hours.

3. THE DOWNBURST THUNDERSTORM ON RADAR AND SATELLITE

Fujita (1978) observed that the downburst storm has signatures that can be identified on radar and satellite: the bow echo and a warm spot on cloud top. The Springfield echo exhibited these signatures in classic form.

Fujita (1978) described three stages of the life cycle of the bow echo. In its first stage it is merely a large, strong, and tall echo. In its second stage the central portion of the echo accelerates ahead of the remainder of the echo, forming a bow-shaped arc of echo. Damaging winds (downbursts) develop on the leading edge of the bow. In its final stage the echo complex evolves into a comma shape. The head of the comma appears to be the center of rotation of the echo complex. Most downbursts cease in the early part of this stage. Tornadoes are possible near the rotating head.

The St. Louis, MO (STL) and Marseilles, IL (MMO) radars provided excellent coverage of the life cycle of the Springfield bow echo. Figure 17 presents the evolution of the low-level echo.

A developing echo complex, referred to as A, is shown at 1805 GMT. At 1832 a new echo, echo B, entered the scope to the west of echo A. By studying the sequence of radar data, it was apparent that echo B moved faster than A and caught up to A about 1941 GMT. About this time echo A began to grow rapidly, perhaps related to the merger. It is interesting to note that echo B itself resembled a bow echo. Whether damaging winds occurred from B was not confirmed.

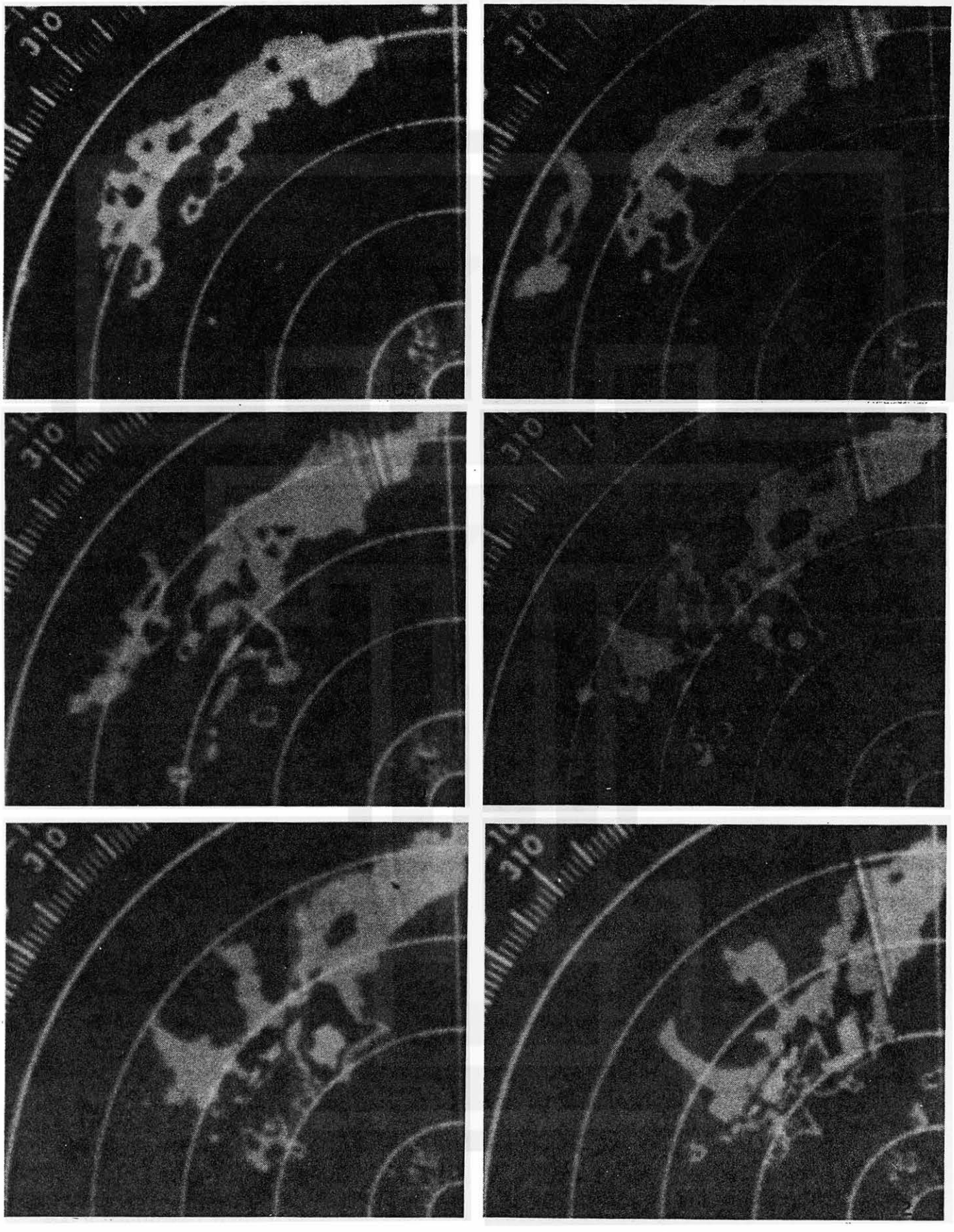

Figure 17. The Springfield bow echo on St. Louis radar. Edges of the photos are oriented N-S and E-W with the center of the scan at lower right. Range marks are at 25 n.mi. intervals.

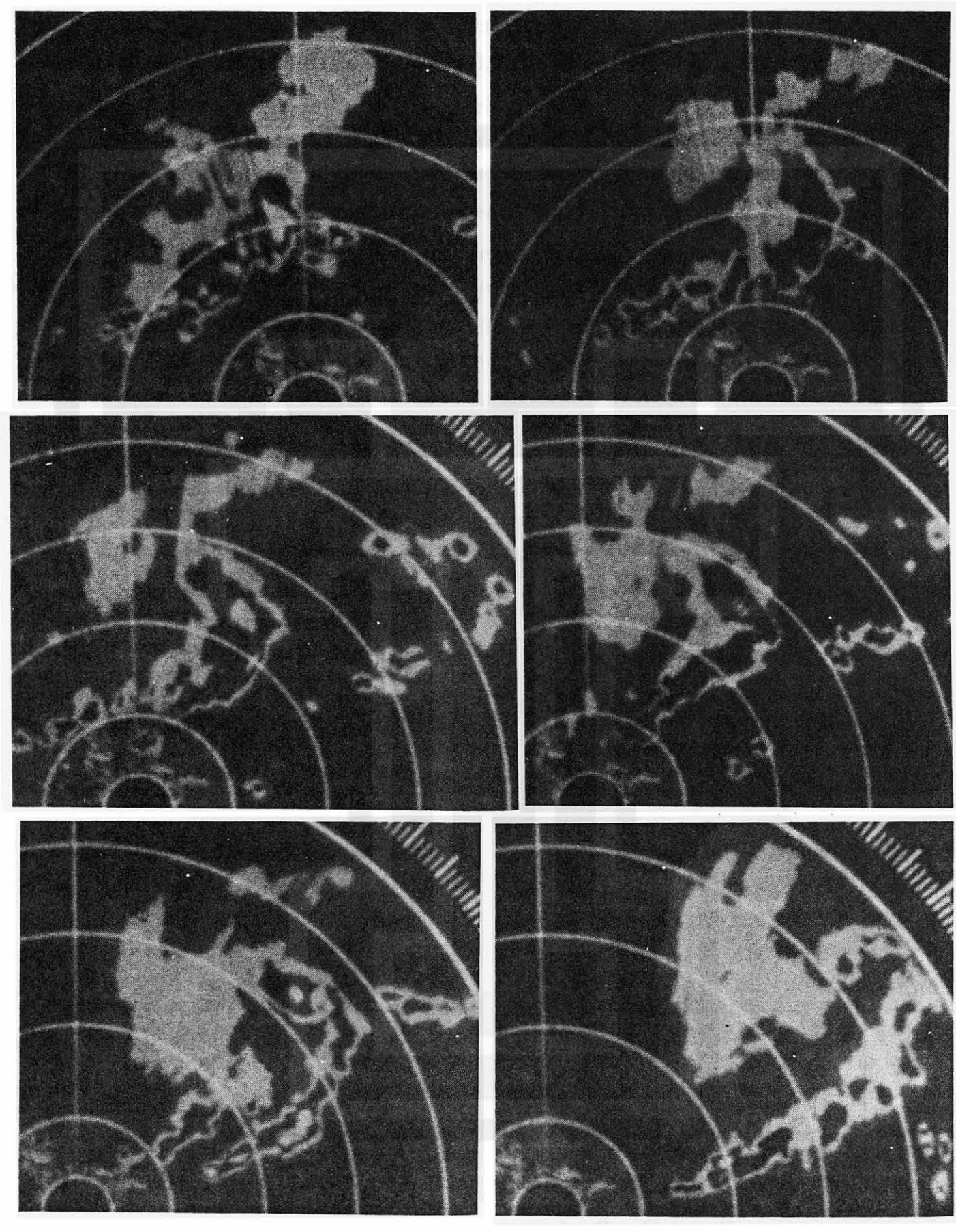

Figure 17, continued. The Springfield bow echo on St. Louis radar. The bottom edge of the photos is oriented E-W through the center of the scan.

By 2106 GMT the echo complex took on a classic bow configuration. Damage began about 2115 GMT, peaked about 2150 GMT, and ended about 2235 GMT. The 2148 GMT radar echo is a bow echo in an advanced stage. Tornadoes 9, 10, 11, and 12 occurred about this time.

At 2222 GMT the comma echo is well developed. By this time the tornado and downburst activity had mostly ceased. The comma echo began to disintegrate at 2306 GMT.

Fujita's (1978) downburst signature on satellite imagery was also demonstrated well by the Springfield storm. Figure 18 presents the development of a warm spot at cloud top which characterizes the downburst stage. The warming occurs just behind the bow echo and appears to indicate sinking.

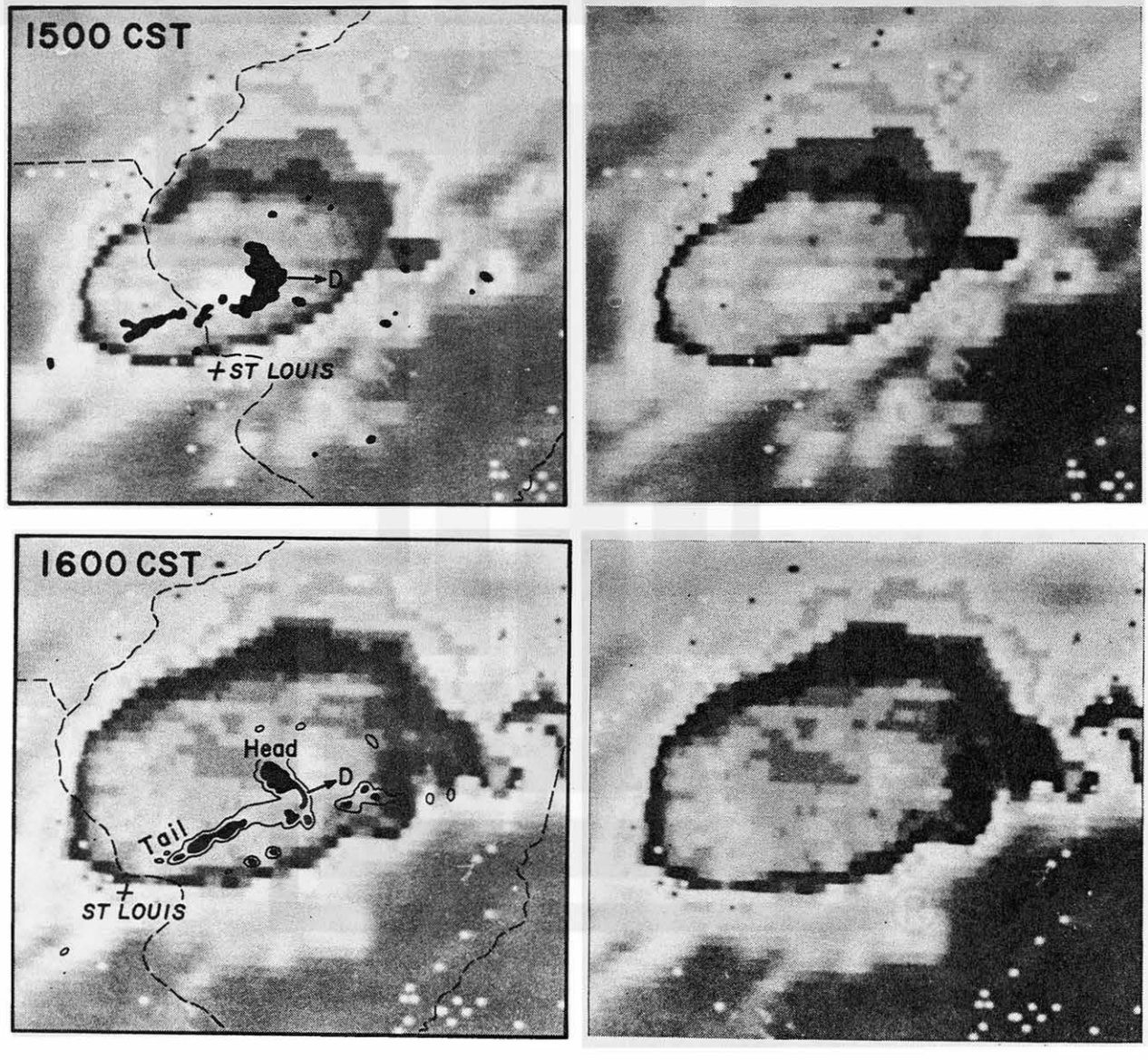

Figure 18. The Springfield storm complex on IR imagery. From Fujita (1978).

4. DESCRIPTION OF DAMAGE

With the exception of the Glenwood Park tornado (9), tornadoes caused relatively little damage to structures. Downburst 9 caused minor damage to several structures, as indicated by damage streaks in Fig. 1. Winds were so strong in this F1 area that residents were sure that they were hit by a tornado.

Damage was primarily to crops. This allowed for a detailed analysis of the damaging wind direction, as denoted by crop fall. The intensity of crop damage, however, is a function of not only the type of crop, but also its age, orientation, and even the brand of seed used. Figure 19 shows two adjacent cornfields in the Buckhart tornado (18). One field was flattened and demolished and the other only bent.

4.1 Ten Downbursts

The wind from downbursts was described by residents as picking up suddenly, accompanied by blinding rain in sheets, and lasting up to about a half hour. Hail was either non-existent or insignificant.

Individual downbursts ranged in width from about 0.5 mi (0.8 km) near the indicated downburst center to as much as 5 miles (8 km) far downstream. The downstream extent of individual downbursts varied from 4 to 9 miles (6 - 14 km).

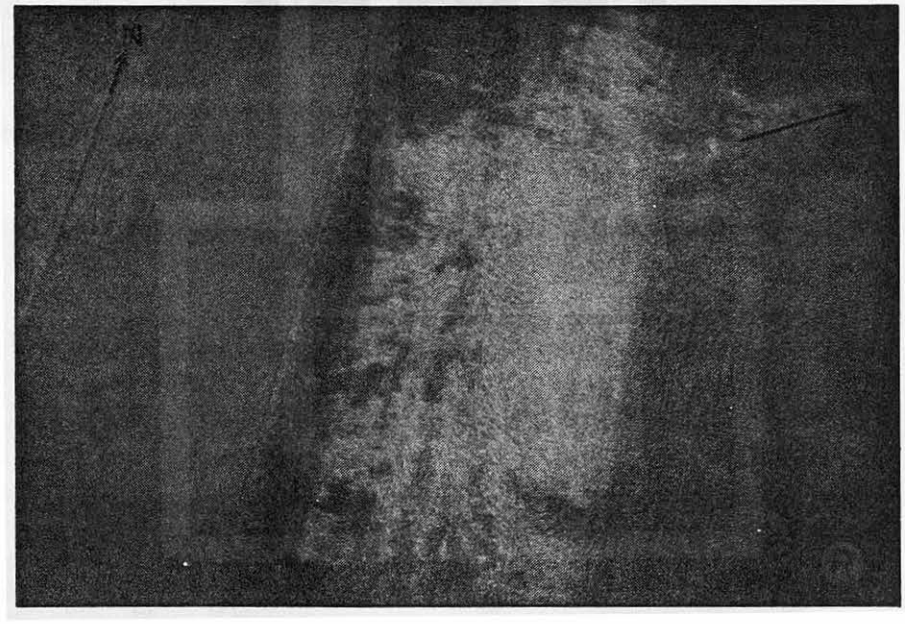

Figure 19. Effect of crop strength upon the damage pattern.

The downbursts caused extensive crop damage. Figure 20 shows leaning corn caused by relatively weak westerly downburst winds. In strong cases the corn was flattened. The damage of Figure 20 occurred from DB 2, 2.5 miles (4 km) northwest of Franklin and 3.5 mi (5.6 km) west of the edge of Map 1.

The most extensive and most destructive downburst was DB 9. It flattened corn and caused considerable property damage all along its path. At least 10 structures were damaged. A tractor trailer was blown off I-55 near the downburst axis.

Figure 21 illustrates the extent and organization of the downburst. The change in the shading of the corn is essentially the axis of the downburst, illustrated by differential scattering of light by different orientations of corn fall. This corresponds to the F 1 region just east of I-55.

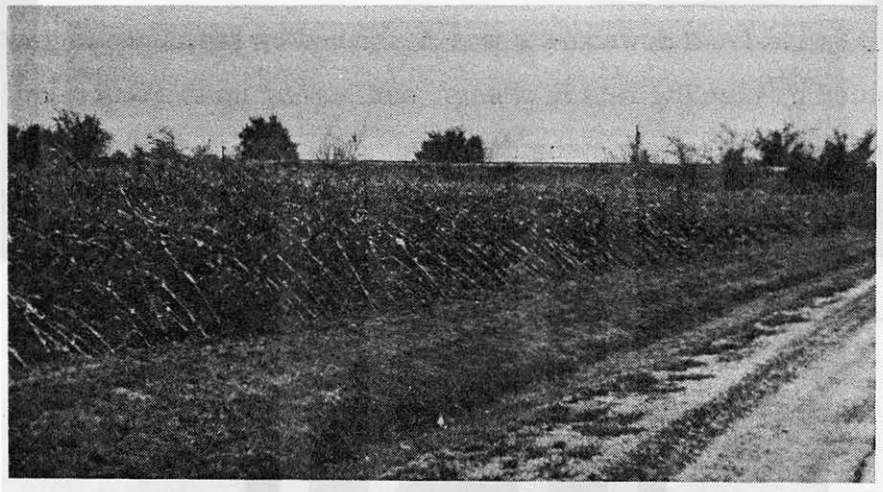

Figure 20. Crop lean caused by relatively weak winds of downburst 2.

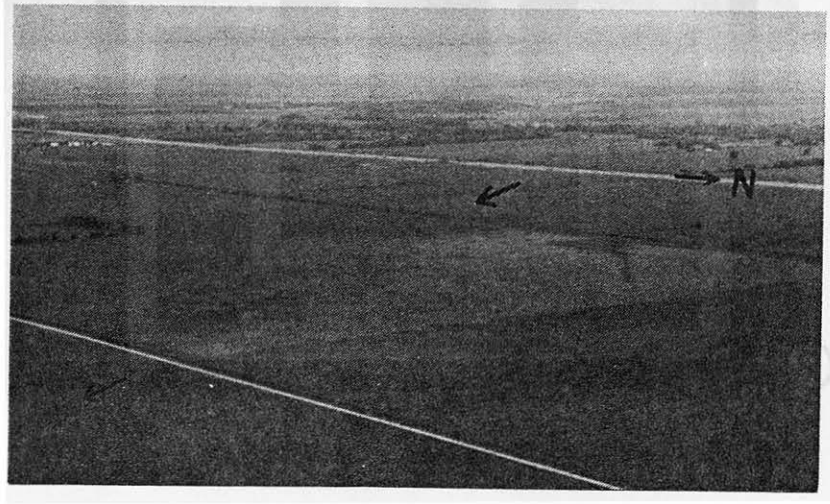

Figure 21. Axis of downburst 9 revealed from crop reflectance.

South of the axis of DB 9 a Cessna 140 crashed at the location shown on Fig. 1, just east of I-55, landing upside down. Its crash site is revealed in Figure 22. Eyewitnesses just north of the crash site said that the plane "buzzed" the highway during a heavy rainstorm and "a great big gust of wind came and flipped it over and over. Then it started coming down." The aircraft was headed southwestward toward St. Louis while returning from an air show at Oshkosh, Wisconsin. A second aircraft, a twin-engine Apache, made an emergency landing on U.S. 36 about 10 mi (16 km) east of Jacksonville during heavy turbulence. This location is just west of the edge of Fig. 1, near the northern edge of downburst damage. These accounts of aircraft mishaps were obtained from Ryan (1977).

Confluent patterns were occasionally seen at the junction of adjacent downbursts or microbursts. Figure 23 is the best example, at the junction of DB 7 and m 7, north of Auburn. There was no evidence of the existence of a vortex within the confluent region.

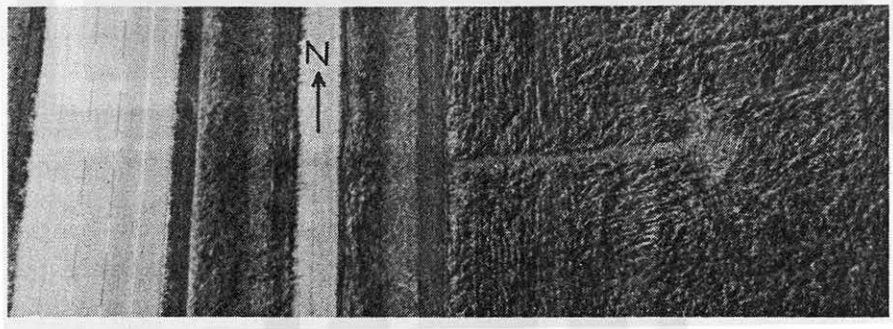

Figure 22. Site of Cessna crash in downburst 9.

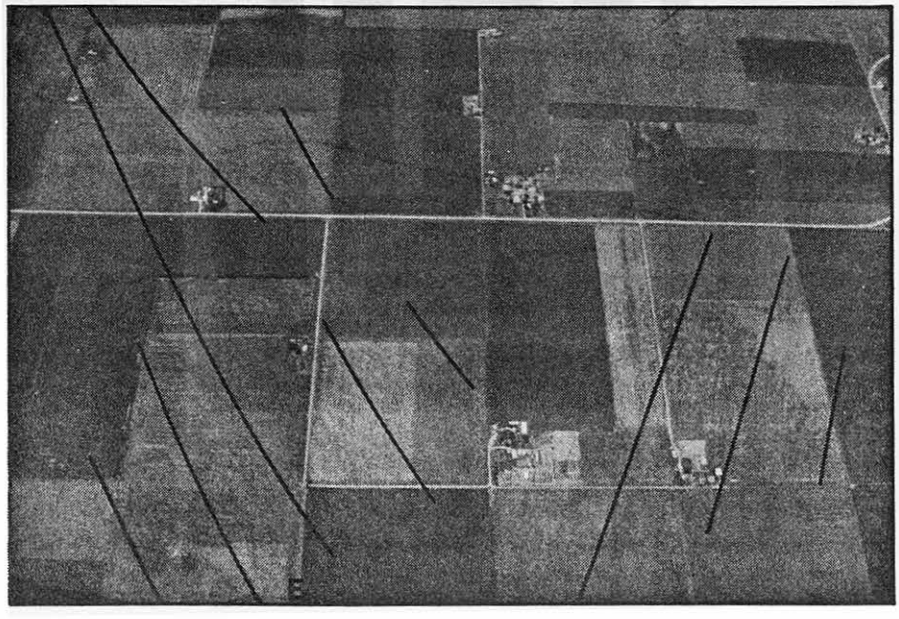

Figure 23. Confluence pattern at the junction of downburst 7 and microburst 7.

Figure 23 reminds one of a photo on the cover of the "Bulletin of the American Meteorological Society," Vol. 58, July 1977. Towery and Morgan (1977) called those streaks "hailstripes," and attributed them to windblown hail. The Springfield survey leads the authors to conclude that similar streaks can be produced without the existence of hail.

4.2 Nineteen Microbursts

By virtue of their compact size, making them visible at a single glance, microbursts are more readily recognized than downbursts. Microbursts were typically less than 1.5 mi (2.4 km) in width and 1 - 3 miles (1.6 - 4.8 km) in downwind extent. F0 damage widths of downbursts were generally twice as wide as those of microbursts.

A classic example of a microburst, m11, is shown in Figure 24, just south of Glenarm. Hatched marks, discussed in Section 5.3 are present on the north edge of the microburst.

Most microbursts were intense enough to cause some type of damage to weak structures. Because of their small size, however, only several actually hit structures.

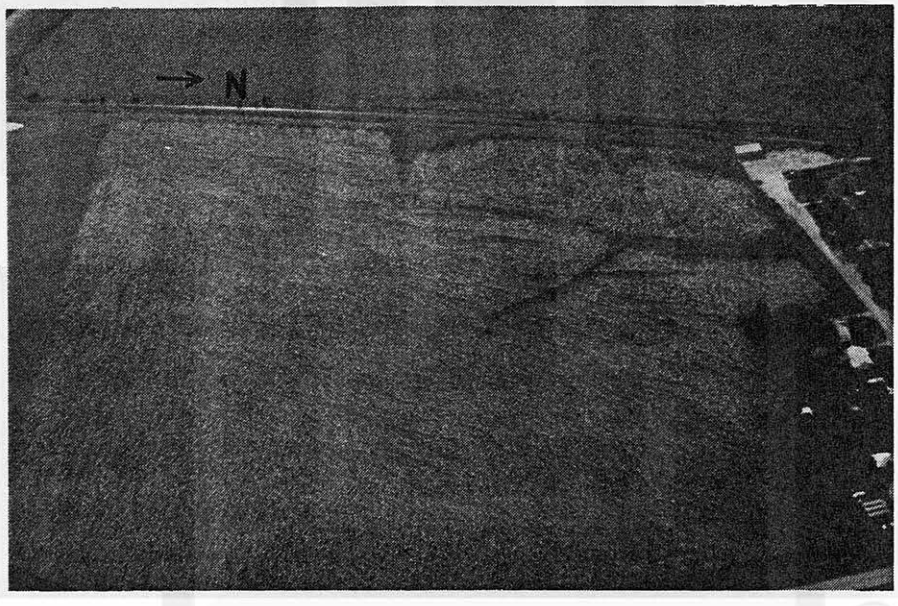

Figure 24. Microburst 11.

4.3 Eighteen Tornadoes

There were 18 small tornadoes embedded within or in the vicinity of the downburst area. One of the tornadoes (no. 11) was anticyclonic (refer to Section 5.7). F PP classifications of these tornadoes are given in Table 1.

TABLE 1

F P P CLASSIFICATIONS OF THE 18 SPRINGFIELD-AREA TORNADOES OF 6 AUGUST 1977

	Name	F	P_L	P_W
1	Auburn	1	2	2
2	Waverly	0	0	3
3	Maxwell	0	0	0
4	Thayer	1	2	1
5	Loami Township	1	1	3
6	Divernon	1	2	2
7	South Fork	2	2	3
8	Twin	1	1	1
9	Glenwood Park	3	2	2
10	Brush Creek	1	2	2
11	Brush Creek Anticyclonic	0	0	0
12	Ball School	0	0	1
13	Beamington	0	0	0
14	Pawnee	1	2	1
15	New City	1	1	1
16	Lake Kincaid	0	1	0
17	Breckenridge	1	1	1
18	Buckhart	1	2	3

All of the tornadoes were revealed best by swaths in the cornfields, as shown in Figure 25. Often the tornadoes were not strong enough to damage structures, as shown. Some of the tornadoes were strong enough to make looping marks, but most only left a wobbly line (a lineation mark) through the fields. Corn was generally erect on either side of the lineation mark (in the absence of a strong downburst) and flattened and slightly confluent (about 30 degrees) within it. For an explanation of the different types of suction swaths, refer to Fujita, Forbes, and Umenhofer (1976).

Figure 26 illustrates the narrow extent of the damaging tornado winds. The Thayer tornado (4) passed through the row of poplar trees toward the sheds. Mrs. Linda Hacker was home at the time of the tornado, and witnessed a debris cloud

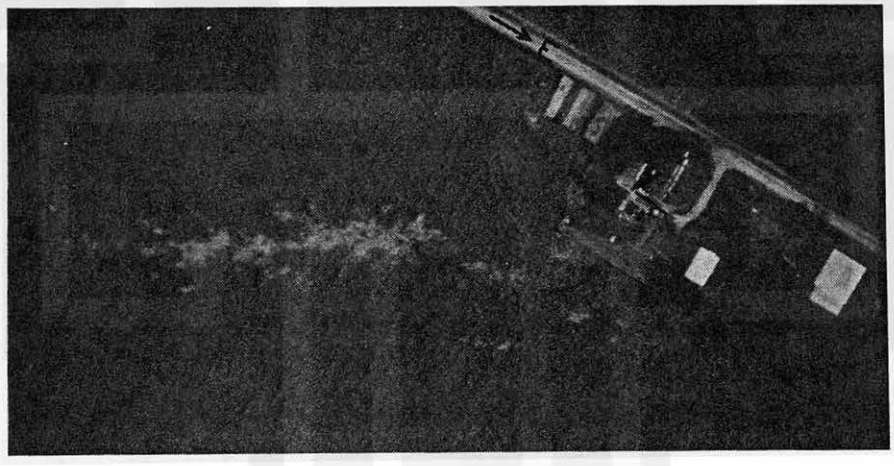

Figure 25. Suction swaths in the Thayer tornado (4). Although the tornado passed over the rightmost building it was not damaged.

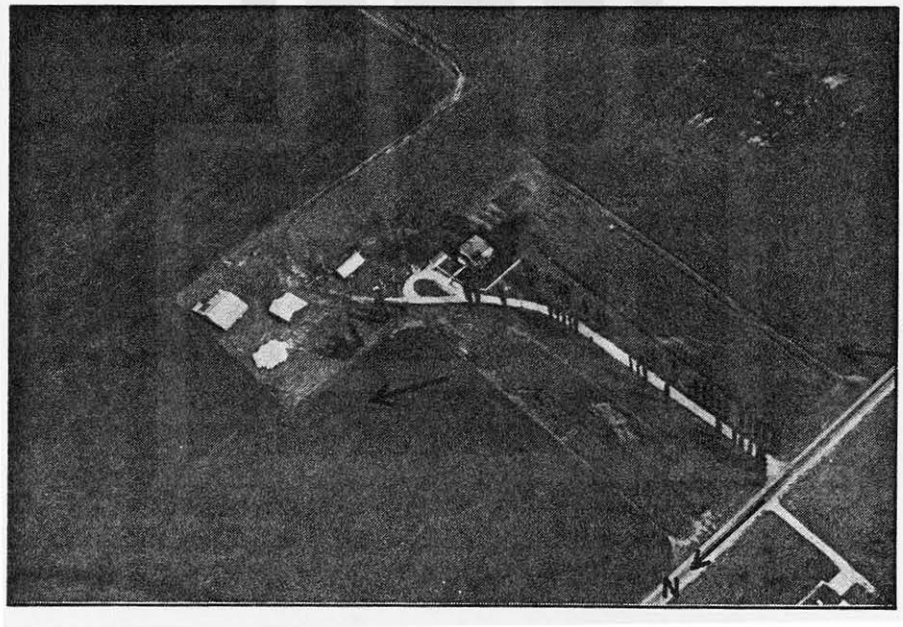

Figure 26. Narrow damage path of the Thayer tornado (4) associated with an observed debris cloud.

and the broken tops of her poplar trees going in circles. No actual funnel cloud was visible. At the time of the tornado she saw rain shafts just to the west, and it rained heavily and became windy just after the tornado hit.

Only 8 of the tornadoes (numbers 4, 6, 9, 10, 14, 15, 17, 18) actually caused any damage to structures. Of these, the Glenwood Park tornado (9) created by far the most damage, and was the strongest (F 3). Figures 27 and 28 illustrate the extent and type of damage done within Glenwood Park. Considerable amounts of debris became airborne, including large portions of roofs. About twenty new and expensive homes were demolished or heavily damaged, and up to twenty others sustained damage.

There were a few spots of damage (A and B of Fig. 27) to the south of the Glenwood Park tornado which were probably caused by the microburst winds of m 9. As shown in Figure 29, a house (apparently under construction) was levelled at A.

The tornado appeared to be disrupted as it passed through a cluster of trees on the north edge of Glenwood Park. It then struck a farm and finally turned left and dissipated while making the looping marks shown in Figure 30.

Figure 27. Path of the tornado (9) through Glenwood Park.

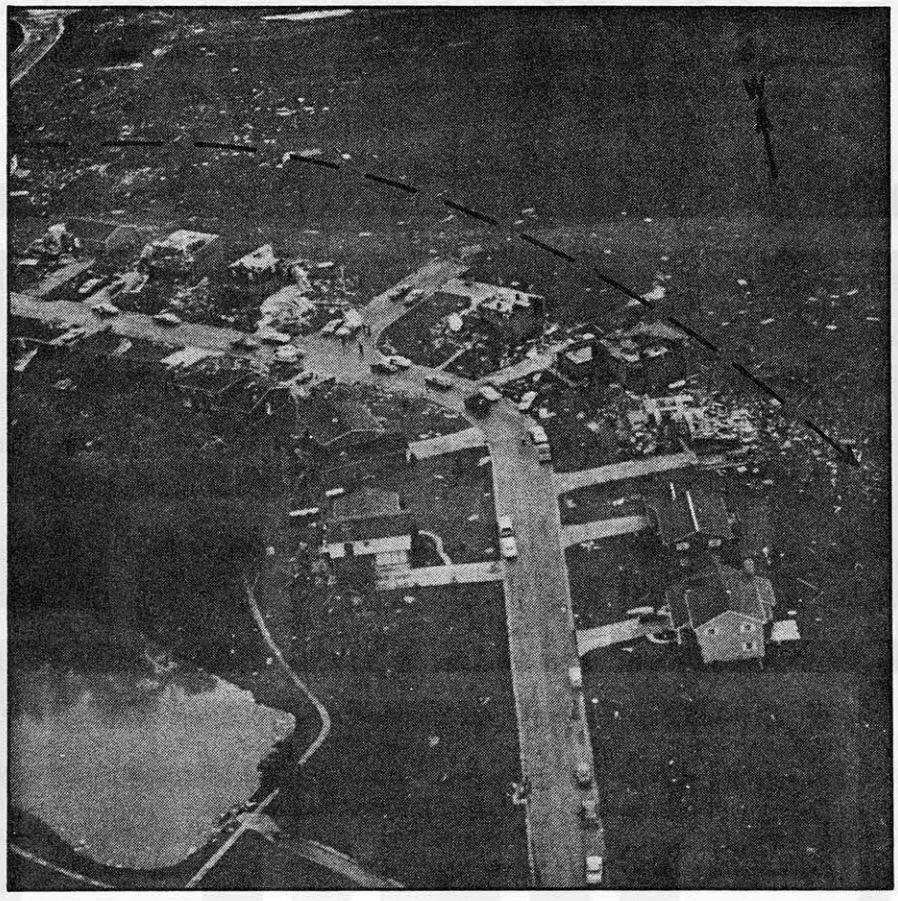

Figure 28. Glenwood Park tornado destroyed homes on one side of the street. Courtesy of the Illinois State Police.

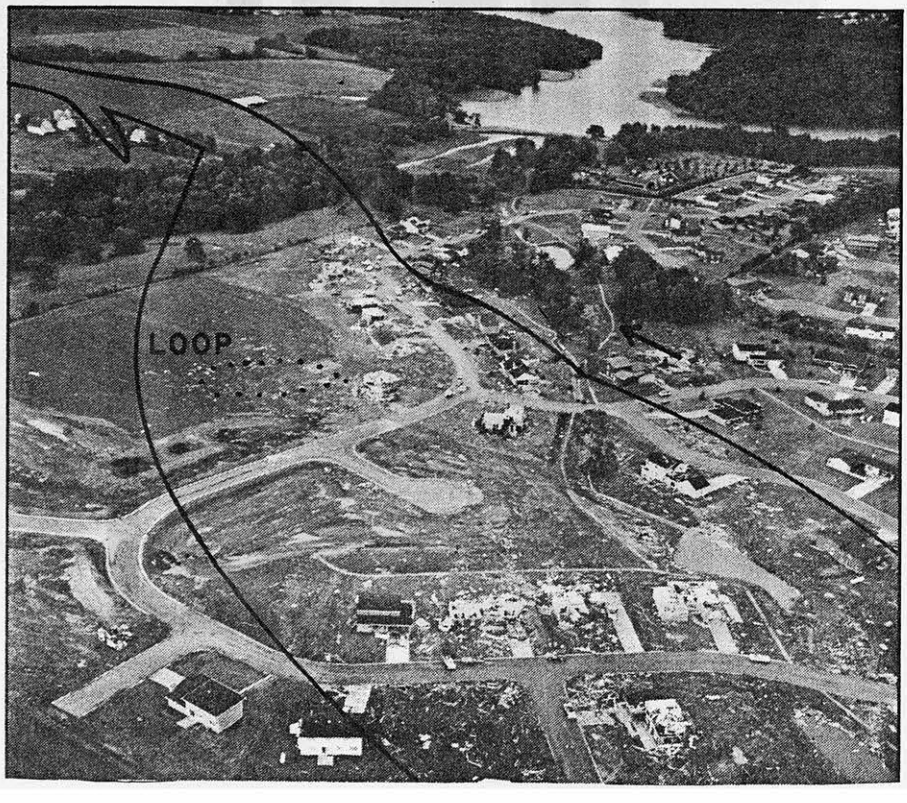

Figure 29. Apparent loop of debris from a house in Glenwood Park.

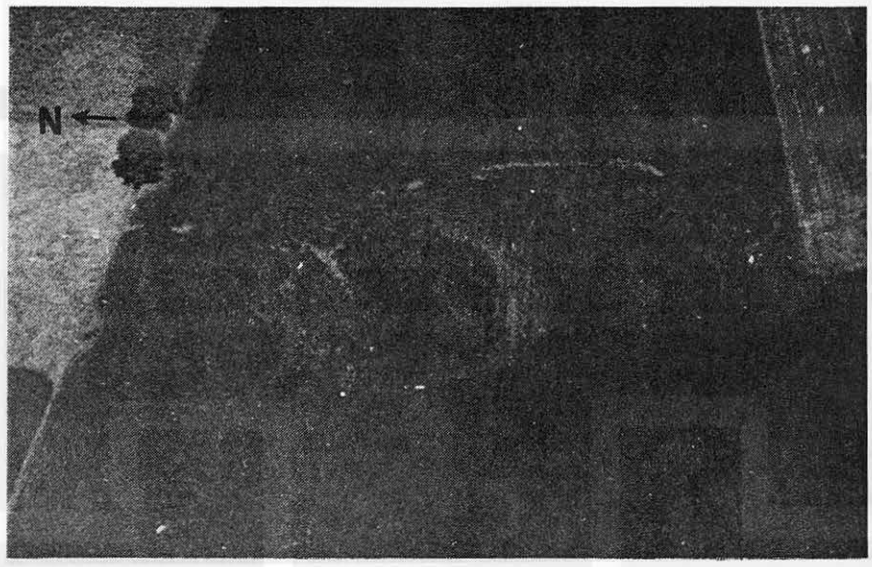

Figure 30. Looping marks during the left turn of the Glenwood Park tornado (9).

Several other tornadoes produced interesting damage patterns. The South Fork tornado (7) had interesting stray suction vortices. Figure 31 is a rectified mapping of their marks (a - c) and looping marks from other vortices.

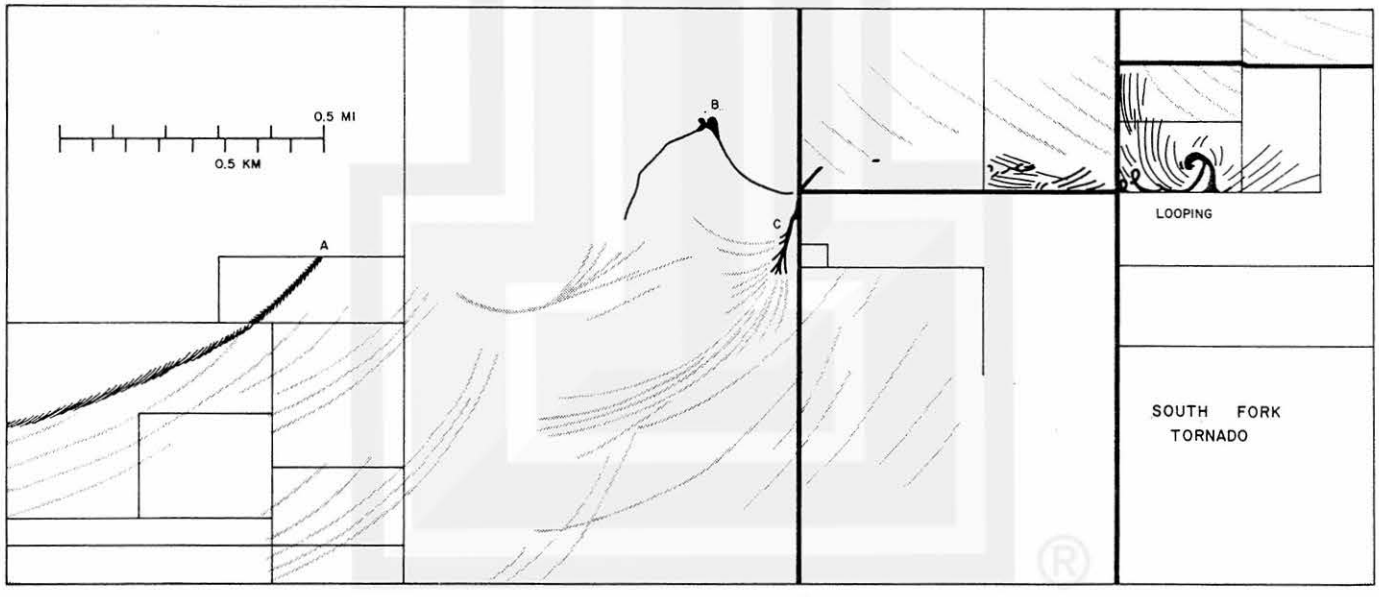

Figure 31. Marks of stray vortices in the South Fork tornado (7).

5. SURFACE MARKS OF DOWNBURSTS AND TORNADOES

Examples of the broad or overall damage patterns from winds of downbursts, microbursts, and tornadoes have been presented in Section 4. This section focuses primarily on the small-scale features within these patterns.

5.1 Tree Wakes, Wake Vortices, Bernoulli Effect, Transverse Markings

From the air there is occasionally some ambiguity in determining the downburst direction, particularly in determining between a direction and its 180 degree opposite counterpart. In such instances, tree wakes were highly beneficial in determining downburst direction.

Tree wakes were additionally interesting because the wakes often showed hydrodynamic analogies. In addition, broken rows of trees often constricted the flow into a jet through the breaks, reminiscent of Bernoulli flow.

Figure 32 shows the shelterbelt effect of a cluster of trees. To the right (east) of the trees the corn is virtually undisturbed, while the corn north and west of the trees is leaning markedly due to westerly winds.

Figure 33 is a close-up of the area along the northern edge of the cluster of trees in Figure 32. Several anticyclonic eddies, indicating the presence of wake vortices, appear to have occurred in the shear along the edge of the wake region. This occurred in downburst 4.

Figure 32. The shelterbelt effect.

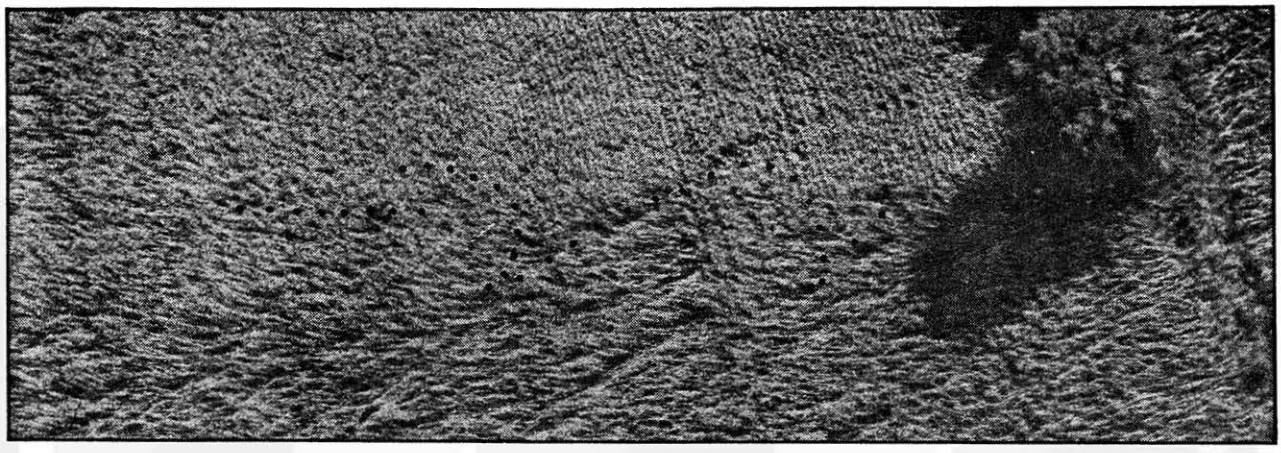

Figure 33. Wake vortices associated with the shelterbelt.

Figure 34 illustrates a break in a tree row where flow was constricted, a Bernoulli effect. Actually, the wind initially may have had a maxima at this location, uprooting the trees at this spot. Thereafter, the jet became exceptionally diffluent, as seen in Figure 35. Figure 35 shows "transverse markings" along the northern edge of the diffluent jet. This occurred in downburst 9.

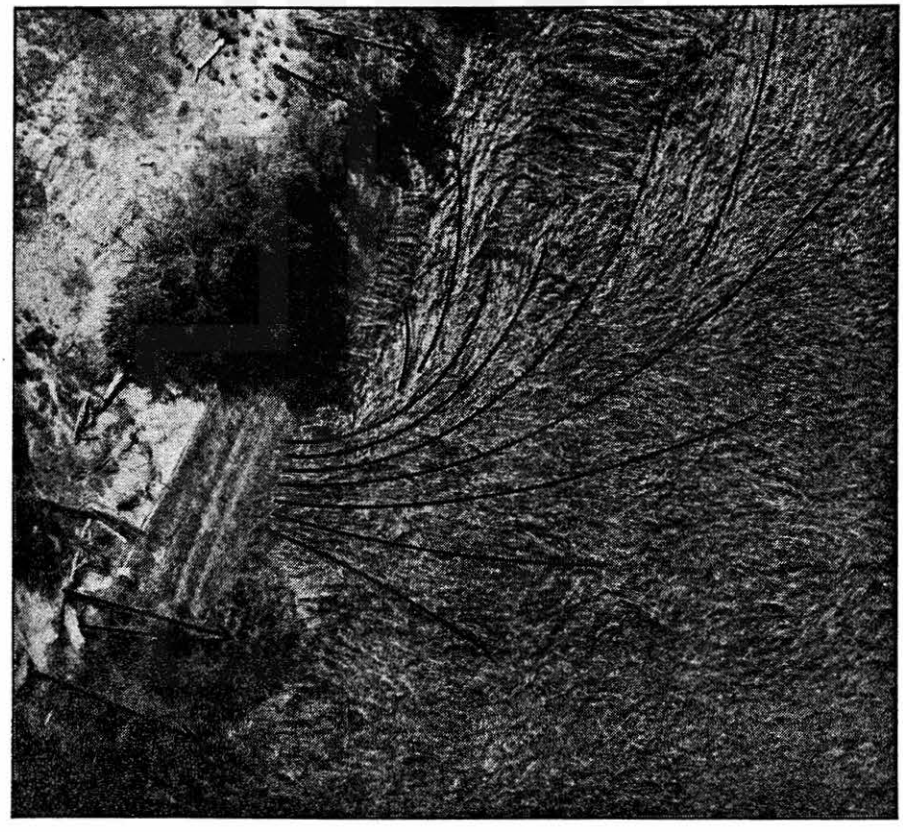

Figure 34. Jet-like winds where flow was constricted--a Bernoulli effect.

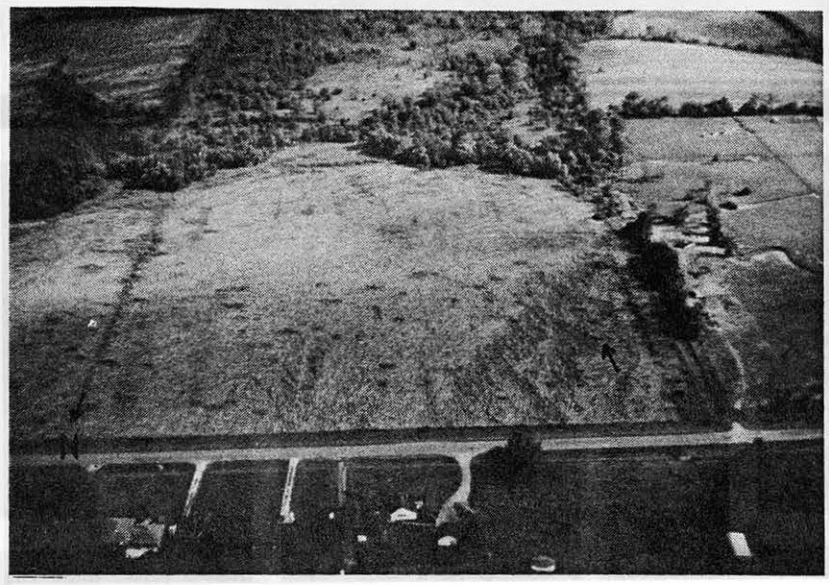

Figure 35. Transverse markings on the edge of the "diffluent jet".

Figure 36 shows a complicated pattern of tree effects within the vicinity of the Divernon tornado (6). At the south edge of the tree row (A) there is a typical wake effect. To the west of this tree row (B) a swirl mark locates the weak vortex of the disorganized Divernon tornado. The row of trees disrupts the vortex as it attempts to cross. Between the tree rows the vortex attempts to re-intensify. Extensive damage occurs at C, where the tree intersection appears to have either constricted the downburst flow, trapped the vortex, or both. Figure 37 shows a close-up of this spot.

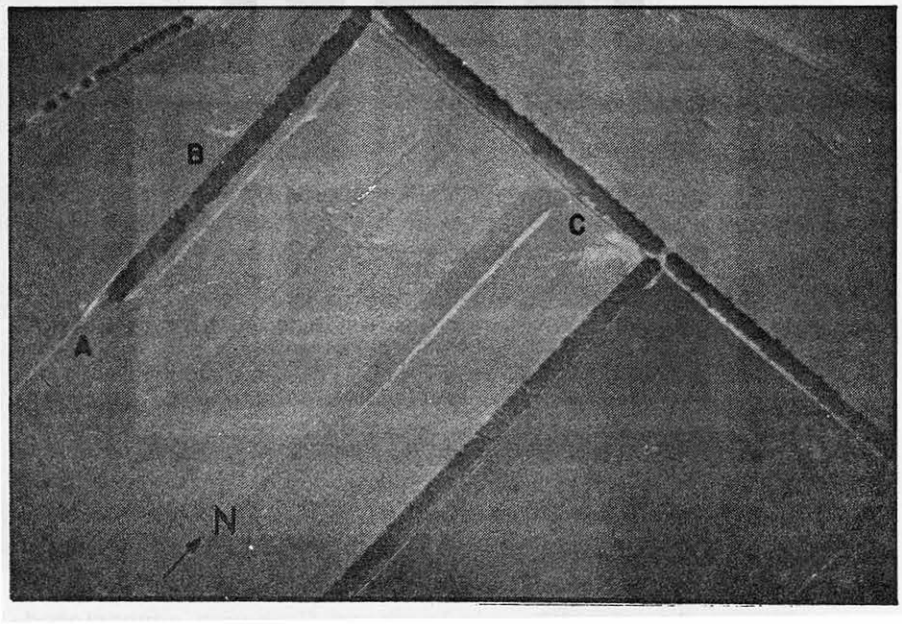

Figure 36. Effect of trees on the Divernon tornado (6).

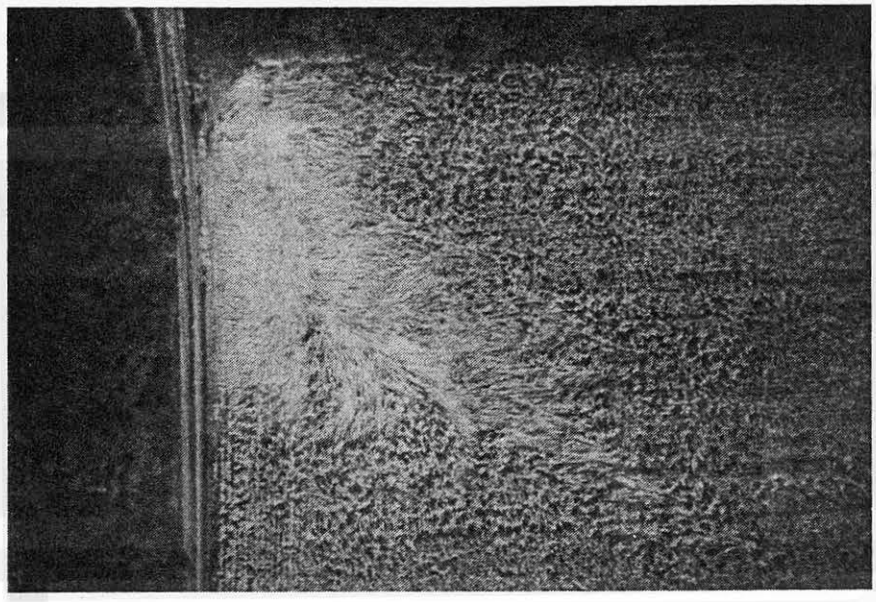

Figure 37. Extensive corn damage near the intersection of tree rows.

5.2 Obstacle-induced Eddies, Swirl Marks

Figures 32 and 33 showed that wake vortices, similar to the von Karman type, were induced at the edge of a row of trees. Eddies of a slightly different nature were also observed.

Figure 38 gives an overall view of the confluent region between microbursts m 10 and m 18. A typical tree wake occurs at the north end of the row of trees (A). At

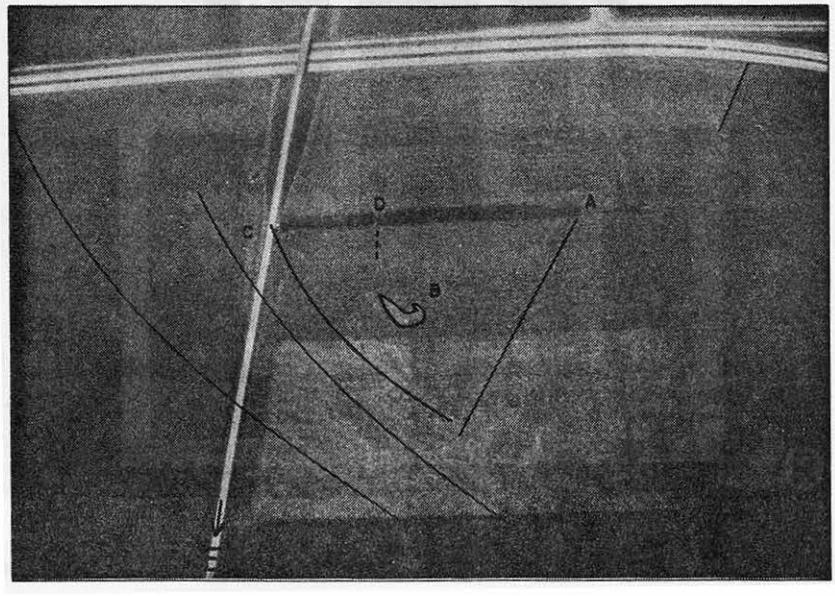

Figure 38. Confluent region between microbursts 10 and 18.

B, however, a distinct swirl can be detected. Figure 39 shows that this eddy was apparently triggered from the sum of three vorticity sources: (1) the shear along the northern edge of microburst m 10; (2) the added shear from the wake effect at C; and (3) shear from a weak jet due to Bernoulli flow through a slight gap in the trees at D.

Other eddies were found in the vicinity of the Beamington (13) and Loami Township (5) tornadoes, but were not so clearly related to obstacles.

5.3 Hatched Marks

Small-scale versions of the transverse marks of Figure 35 were commonly observed within microbursts. These small scale transverse markings were termed "hatched marks". Figure 40 gives a good example from microburst m 6. These hatched marks occurred near the left edge of the microbursts, as in Figure 41 from microburst m 11.

It is not clear whether the hatched and transverse markings are related to shedding of vortices on the left side of the microburst "jet" (i.e., due to the vertical component of vorticity) or due to a rolling motion associated with vertical shear (i.e., due to the horizontal component of vorticity).

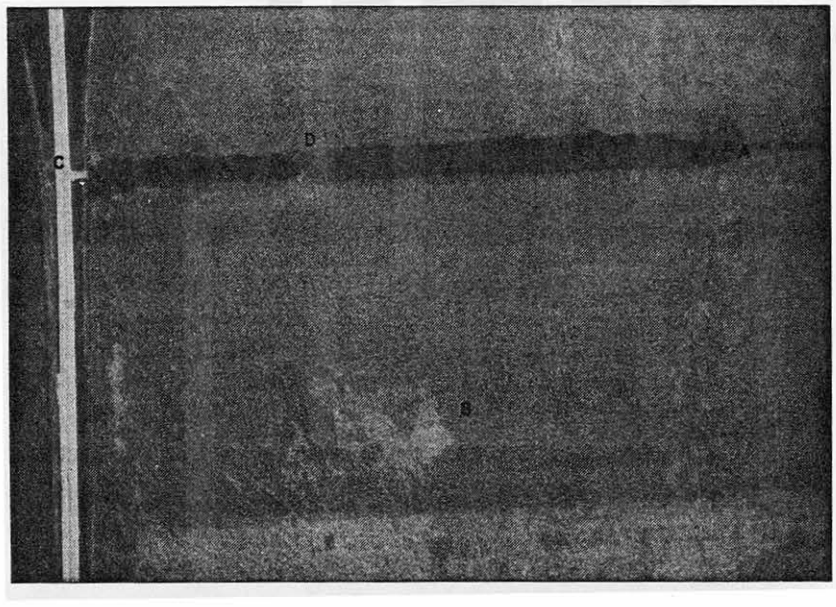

Figure 39. Eddy induced by microbursts and effects of trees.

Figure 40. Hatched marks in microburst 6.

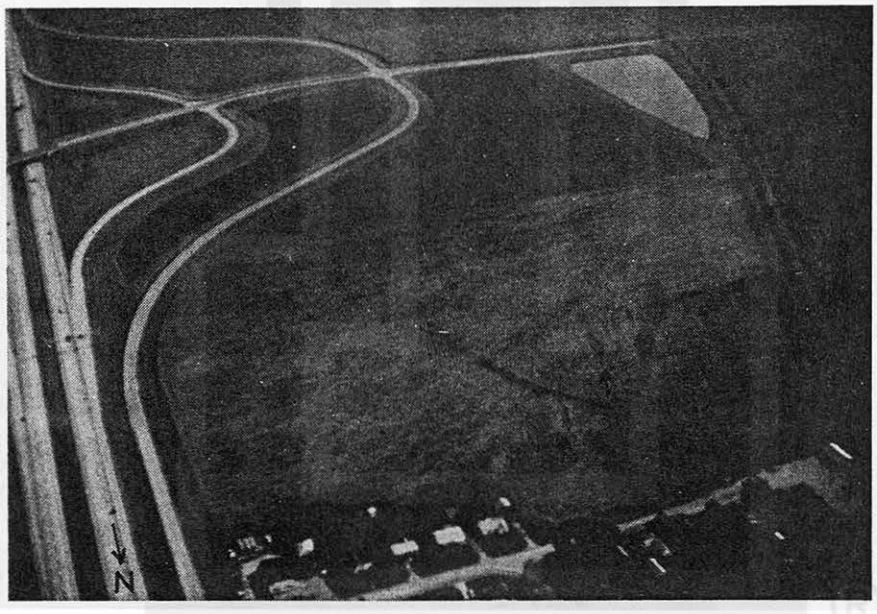

Figure 41. Hatched marks in microburst 11.

5.4 Blow-down Spots

Microbursts did not appear to be the smallest scale of downward flow. There were spots on the scale of 10 m in diameter in which corn was flattened. These occurred both in the presence and absence of downburst/microburst flow, and were termed "blow-down spots". Figure 42 shows two blow-down spots embedded within the relatively weak southerly flow south of the Auburn tornado (1). Other blow-down spots were observed immediately (20 m) south of the Twin tornado (8), and near the beginning of the Glenwood Park tornado (9).

Evidence is far from conclusive, but the occurrence of blow-down spots in close proximity to the tornado suggests the following mechanism. The blow-down spots occurred in association with small-diameter tornadoes which must have had an exceptionally shallow inflow layer. Similarly, inflow must have come from within an exceptionally small radius of influence. Within the radius of influence air accelerated toward the tornado; outside, the air flowed undisturbed. Therefore, divergence is likely near the edge of the radius of influence. Continuing this line of reasoning, it is tempting to speculate that the blow-down spots occurred along the edge of this radius of influence where horizontal divergence occurred in the layer nearest the ground, promoting downflow from above.

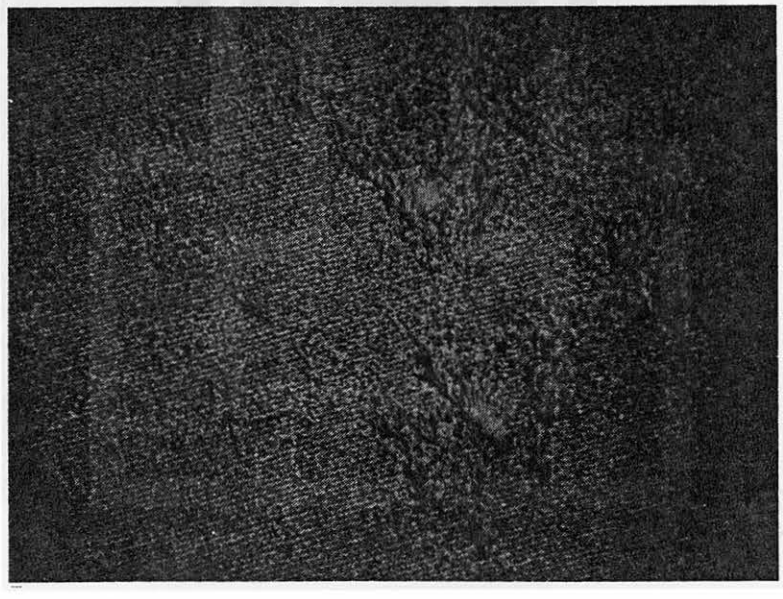

Figure 42. Blow-down spots near the Auburn tornado (1).

5.5 Suction Swaths

A few examples of typical looping and scalloping marks created by tornadoes in the Springfield storm have been shown earlier. A few interesting and, perhaps, uncommon examples are presented here.

Figure 31 presented a mapping of a portion of the South Fork tornado, which contained stray suction vortices. Figure 43 shows that stray vortex b left basically a lineation mark. The vortex, however, apparently moved along an erratic path that made two loops.

The Brush Creek tornado (10) left huge, classic scalloping marks, as shown in Figure 44. The path of the anticyclonic tornado, discussed in Section 5.7, is also visible in the figure.

Several tornadoes left lineation marks. The Breckenridge tornado (17) left a dark lineation mark flanked by bright areas of inflow, Figure 45. This type of pattern has been explained as a pattern of deposition and removal (shown best when only corn stubble is present).

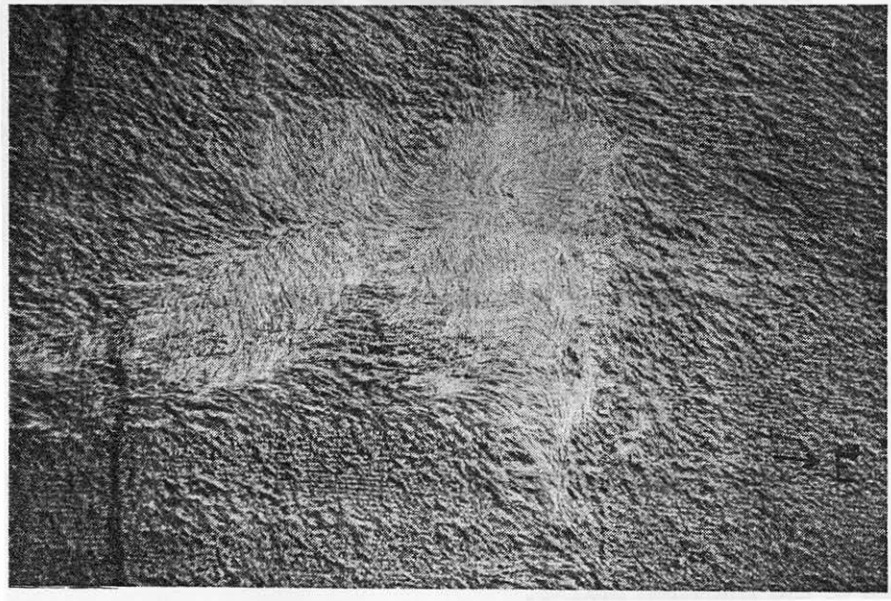

Figure 43. Double loop in the path of a stray vortex of the South Fork tornado (7).

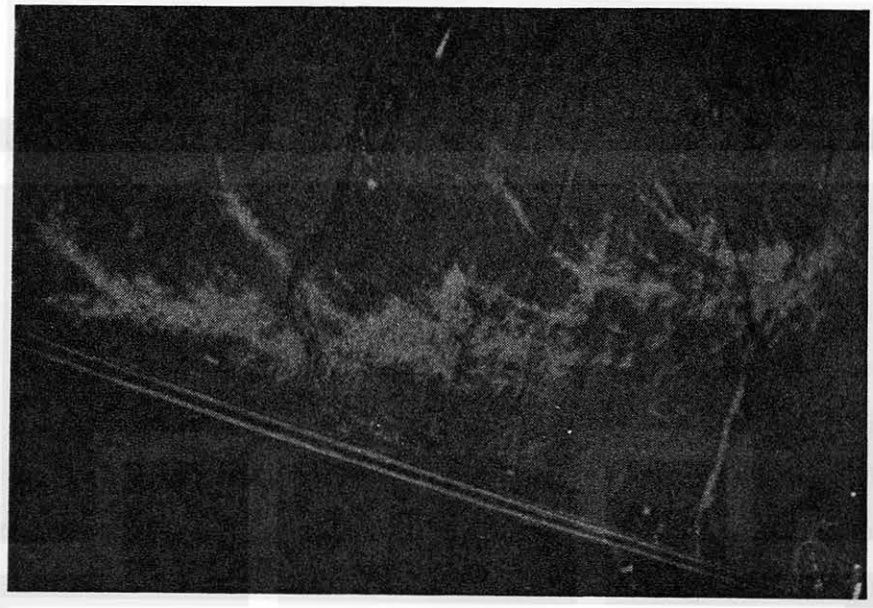

Figure 44. Scalloping marks in the Brush Creek tornado (10).

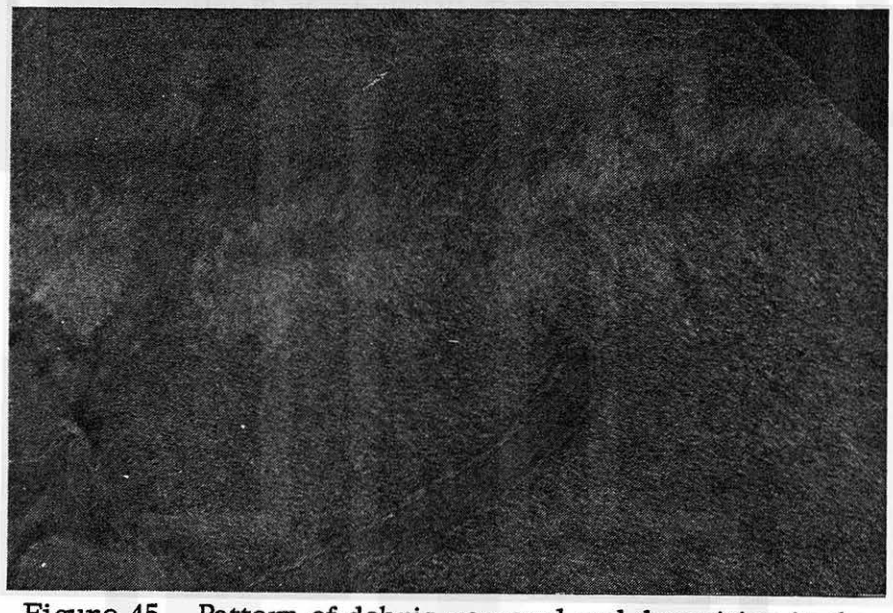

Figure 45. Pattern of debris removal and deposition in the Breckenridge tornado (17).

A pair of lineation marks, left by "twin" suction vortices in the Twin tornado (8), are shown in Figure 46. Also visible are numerous blow-down spots to the south of the lineation marks.

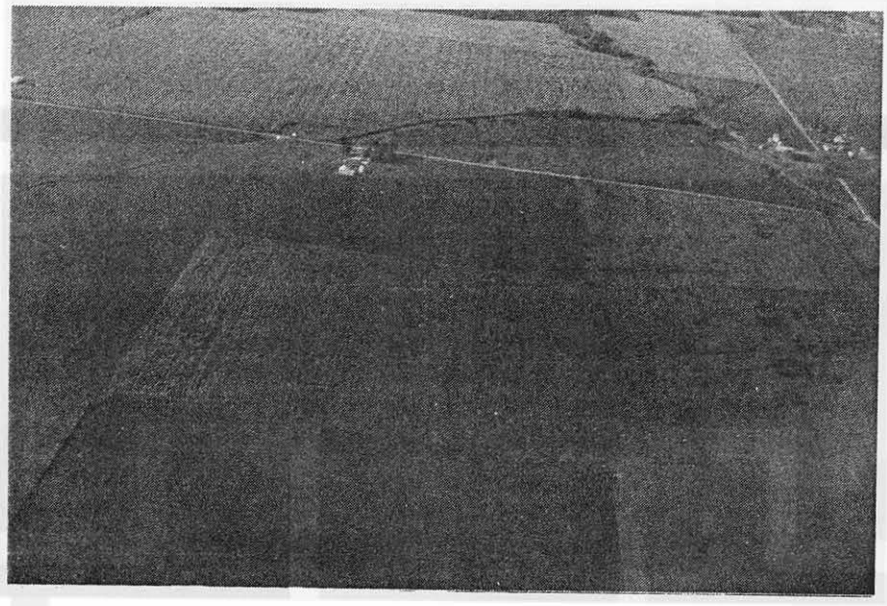

Figure 46. Pair of lineation marks produced by stray suction vortices in the Twin tornado (8).

5.6 Spin-up Marks; Influx Marks

Two types of marks were observed that appeared to imply that vortices were generated by spin-up of vorticity due to low-level convergence, the "spin-up mark" and the "influx mark". Spin-up marks were observed in the South Fork (7) tornado. Influx marks were observed in the Glenwood Park (9), South Fork (7), and Brush Creek (10) tornadoes.

Inasmuch as both spin-up and influx marks were observed within the South Fork tornado (7), the reader may wish to refer again to Figures 2 and 31. Figure 47 gives another view of the three stray suction vortices. Vortex B produced the double-looped lineation mark of Figure 43. Vortex C was associated with a distinct spin-up mark, shown in close-up in Figure 48. Vortex A was associated with an influx mark, discussed later and shown in Figure 49.

It can be seen in Figures 2, 31, 47, and 48 that a swath of minor wind damage swirled toward vortex C from the southwest. In fact, similar swaths occurred "upwind" from the lineation marks of vortices A and B. These swaths were associated with downburst winds.

On the left side of the swaths of downburst winds, vorticity is cyclonic. Figure 48 also implies marked convergence in the region just southwest of the lineation mark. Stretching of vorticity, therefore, appears to be the process which generated vortex C.

Figure 47. Marks of stray vortices in the South Fork tornado (7).

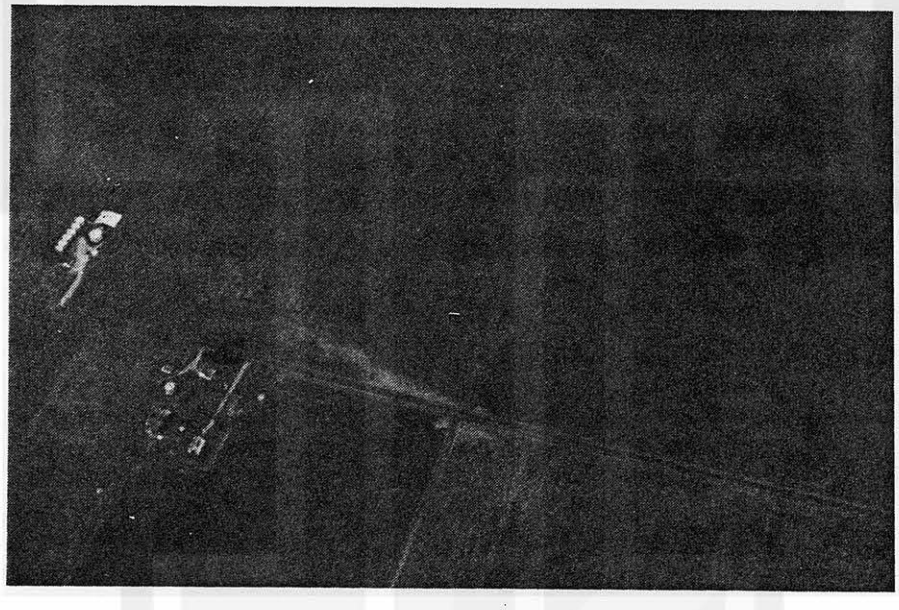

Figure 48. Spin-up mark of vortex C of the South Fork tornado (7).

Influx marks appear to reveal a slower process of generation of vorticity than that shown by spin-up marks. Figure 49 shows the influx marks associated with the development of vortex A of the South Fork tornado (7). The influx marks occurred between the swath of downburst damage and the herringbone pattern or lineation mark of the vortex, while vorticity was increasing to tornado magnitude.

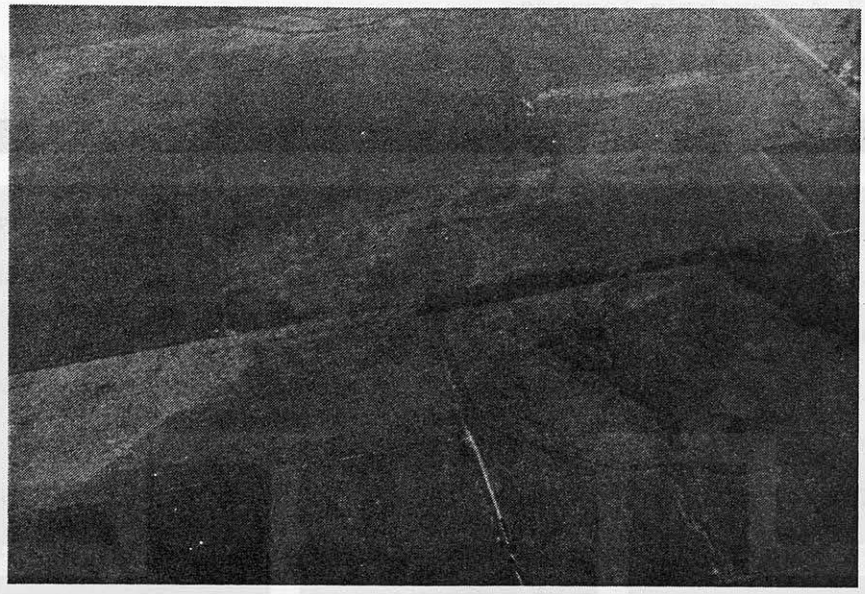

Figure 49. Influx and herringbone marks left by a stray vortex of the South Fork tornado (7).

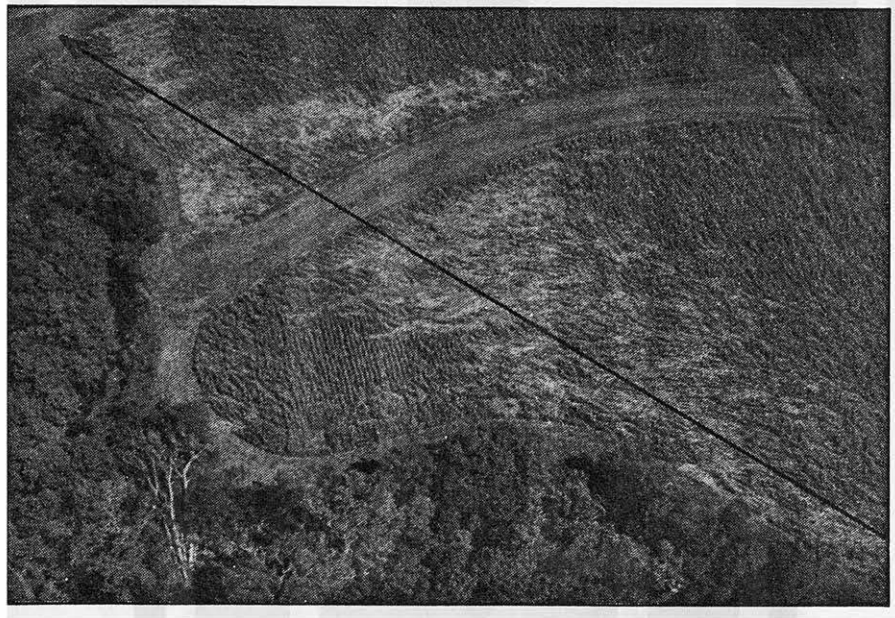

Figure 50. Influx marks left by the Glenwood Park tornado (9) as it intensified near its origin.

Figure 50 shows influx marks near the origin of the Glenwood Park tornado (9). They appear to identify strong inflow and incipient rotation.

5.7 Anticyclonic Tornado

The presence of a confirmed anticyclonic tornado (11) among the Springfield outbreak was mentioned earlier. The path of the tornado was shown in Figures 1 and 44.

Figure 51 shows a ground view of the cornfall, looking northward. Notice that the corn leaning from the southeast lies atop the corn leaning from the southwest. Therefore, the southwest wind preceded the southeast wind as the vortex travelled northward. This implies an anticyclonic tornado, and, indeed, is opposite from the normal sequence of stacking by a cyclonic tornado.

Figure 52 also confirms that the tornado was anticyclonic. The loops can be seen on the right side of the tornado center, opposite that of a northward-moving cyclonic tornado (which would be on the left side).

Figure 51. Cornfall in the Brush Creek anticyclonic tornado (11).

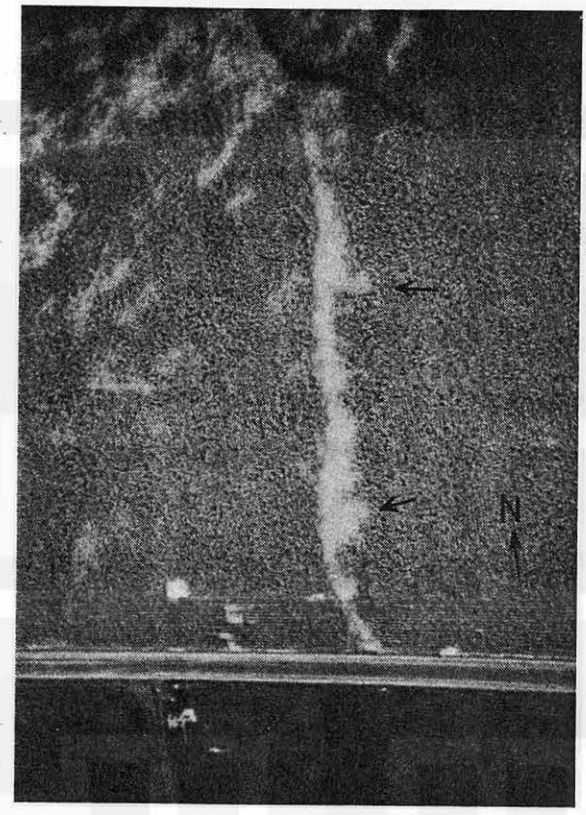

Figure 52. Looping marks in the anticyclonic tornado.

6. RELATION BETWEEN DOWNBURSTS AND TORNADOES

The Thayer tornado (4) was one of only five that are known to have been witnessed (numbers 2, 4, 9, 17, 18). Of these, two possessed debris clouds without funnels (4 and 18). Many of the tornadoes were obscured by torrential rains in their vicinity.

These factors, combined with a substantial duration of winds and rain, allowed times to be pinpointed at only a few locations. Times of downbursts and tornadoes at other locations, shown on Figure 1, were extrapolated from these times and from radar. Such extrapolations were justified through knowledge of the weather sequence at many locations, based upon interviews of residents.

Interviews of residents who witnessed the tornadoes revealed that the tornadoes occurred at the leading edge of the downbursts. Typically, the tornado was succeeded immediately by heavy rains and strong winds. Sometimes it was raining lightly as the tornado passed by.

Section 5.6 indicates that the downbursts and microbursts can supply the vorticity for cyclonic tornado formation on the left side of the downburst. Cyclonic eddies associated with downbursts were shown in Section 5.2.

In the Springfield outbreak, damage surveys and interviews indicated that nearly all of the tornadoes were related to the downbursts and microbursts. On the basis of lack of downburst-related corn damage, tornadoes number 1, 4, 6, 8, 10, 11, 14, 15, and 16 did not appear to be related to substantial downburst winds. However, eyewitnesses revealed that some of these areas experienced strong, but not damaging, thunderstorm winds. Thus, most of the tornadoes probably occurred either in association with downbursts and microbursts or on the leading edge of the gust front.

In addition to apparently triggering tornado formation, microbursts and downbursts have, at times, appeared to be related to intensification of existing tornadoes. One such example is presented in Figure 53, where microburst m 9 occurred near a large suction vortex looping mark within the Glenwood Park tornado (9). The

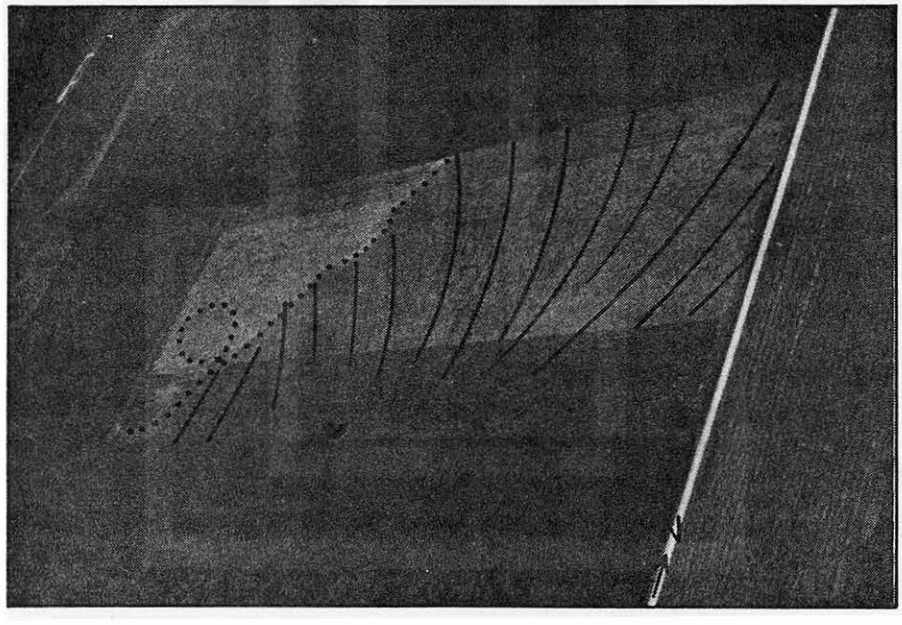

Figure 53. Looping mark within the Glenwood Park tornado (9).

tornado appeared to reach its peak intensity at this location. The microburst is thought to provide additional shear vorticity to the tornado.

Downbursts and microbursts appear to sometimes cause a tornado to turn. In Figure 54, the winds of downburst D5 caused the tiny vortex of the Loami Township tornado (5) to make a right turn toward the southeast. Tornado cyclone winds shown in Figure 55 appeared to cause the Buckhart tornado (18) to make a right turn toward the northeast.

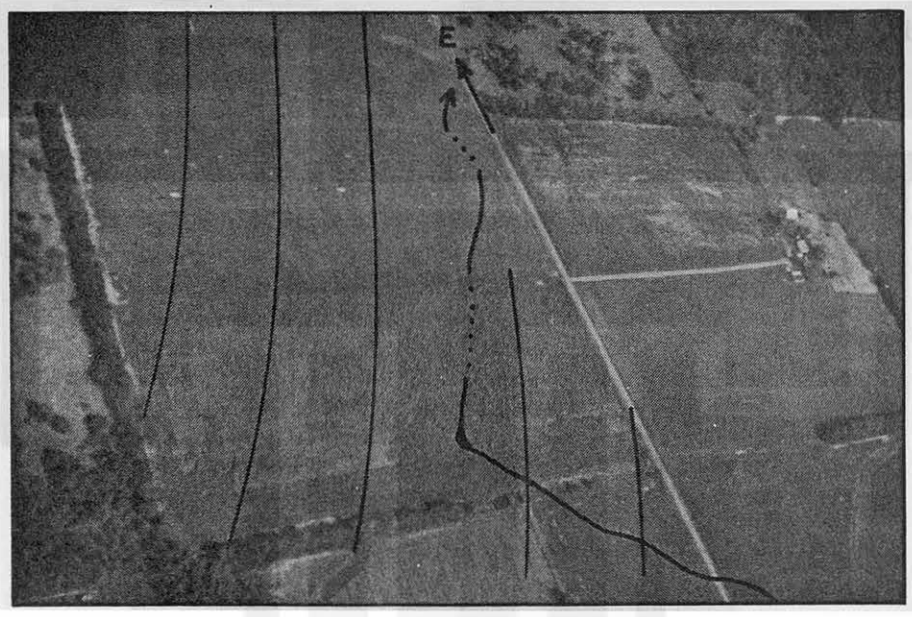

Figure 54. Right turn of a stray vortex of the Loami Township tornado (5).

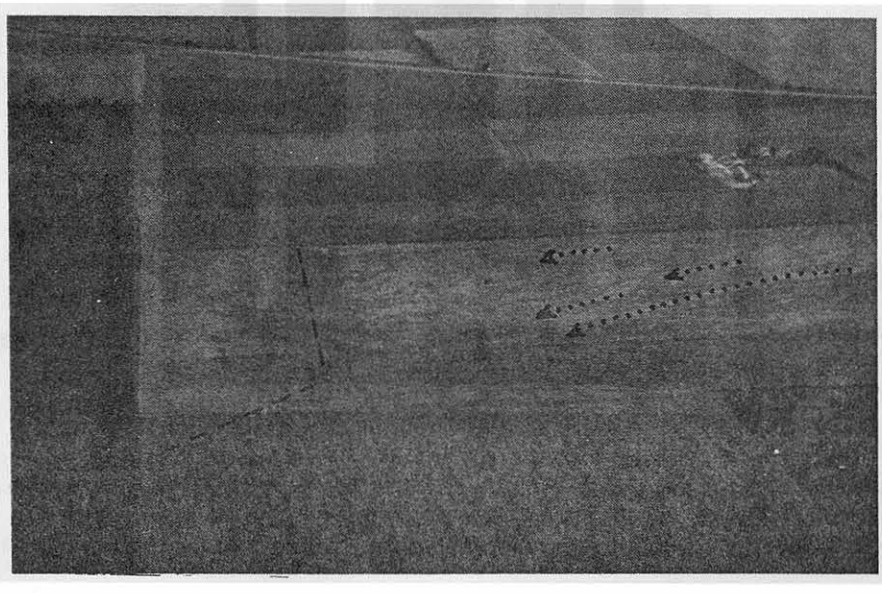

Figure 55. Right turn of the Buckhart tornado (18).

The Glenwood Park tornado (9), initially moving from the southwest, made a spectacular turn immediately after striking Glenwood Park, and lifted while moving toward the northwest. Figures 56 and 57 show its initial southwesterly, quasi-linear path and its curving left turn, respectively. This left turn may have been caused by m 18. In addition to this dramatic left turn, the tornado made small wobbles as it moved northeastward, as shown in Figure 56, perhaps related to fluctuations in strengths of m 8, m 9, and DB 7. Figure 58 is a rectified mapping of the latter 50% of the path.

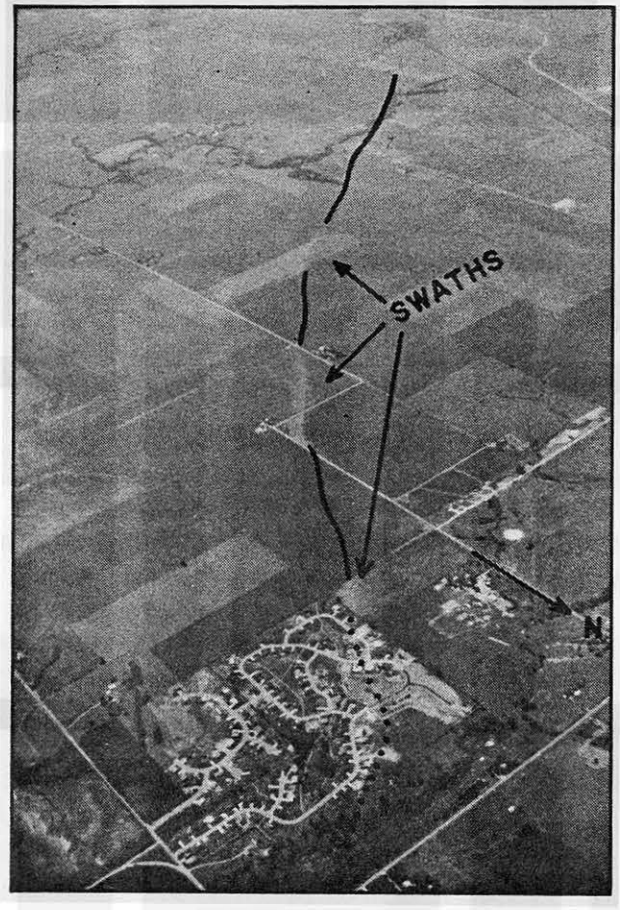

Figure 56. Path of the Glenwood Park tornado (9) before it reached the housing subdivision.

Downbursts and microbursts also appeared to contribute to the disruption or dissipation of several tornadoes. The Pawnee tornado (14) was a good example. Refer to Figure 1.

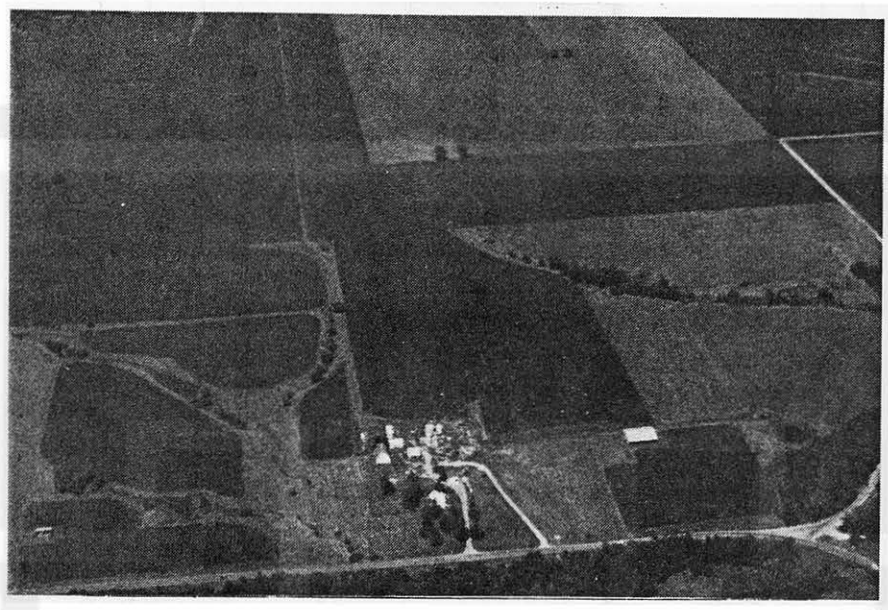

Figure 57. Curving left turn of the Glenwood Park tornado (9).

At first glance, the damage pattern of Figure 1 reveals that the downburst winds blew straight across several tornado paths without any associated tornado turn or disruption. In such cases, the tornadoes apparently occurred in advance of the downburst winds, as was the case near the Breckenridge tornado (17), Figure 59. Here an eyewitness, Mr. William Conboy, revealed that the tornado was accompanied by light rain and light wind. The strong winds of microburst m 16 occurred just after the tornado passed.

7. POSTSCRIPT

The occurrence of 18 tornadoes and several other eddies in such a small area seriously shakes the common concept that at a particular moment a single tornado occurs from a rotating thunderstorm. It also poses some important questions. Do the tornadoes occur with the updrafts of individual thunderstorms? If not, is the stretching supplied by mechanical lifting along the edge of the advancing downburst or gust front? If the latter is the case, how does one distinguish an eddy or other whirlwind from a tornado? Idso (1974) asked similar questions regarding tornadoes and dust devils.

How do we define a tornado?

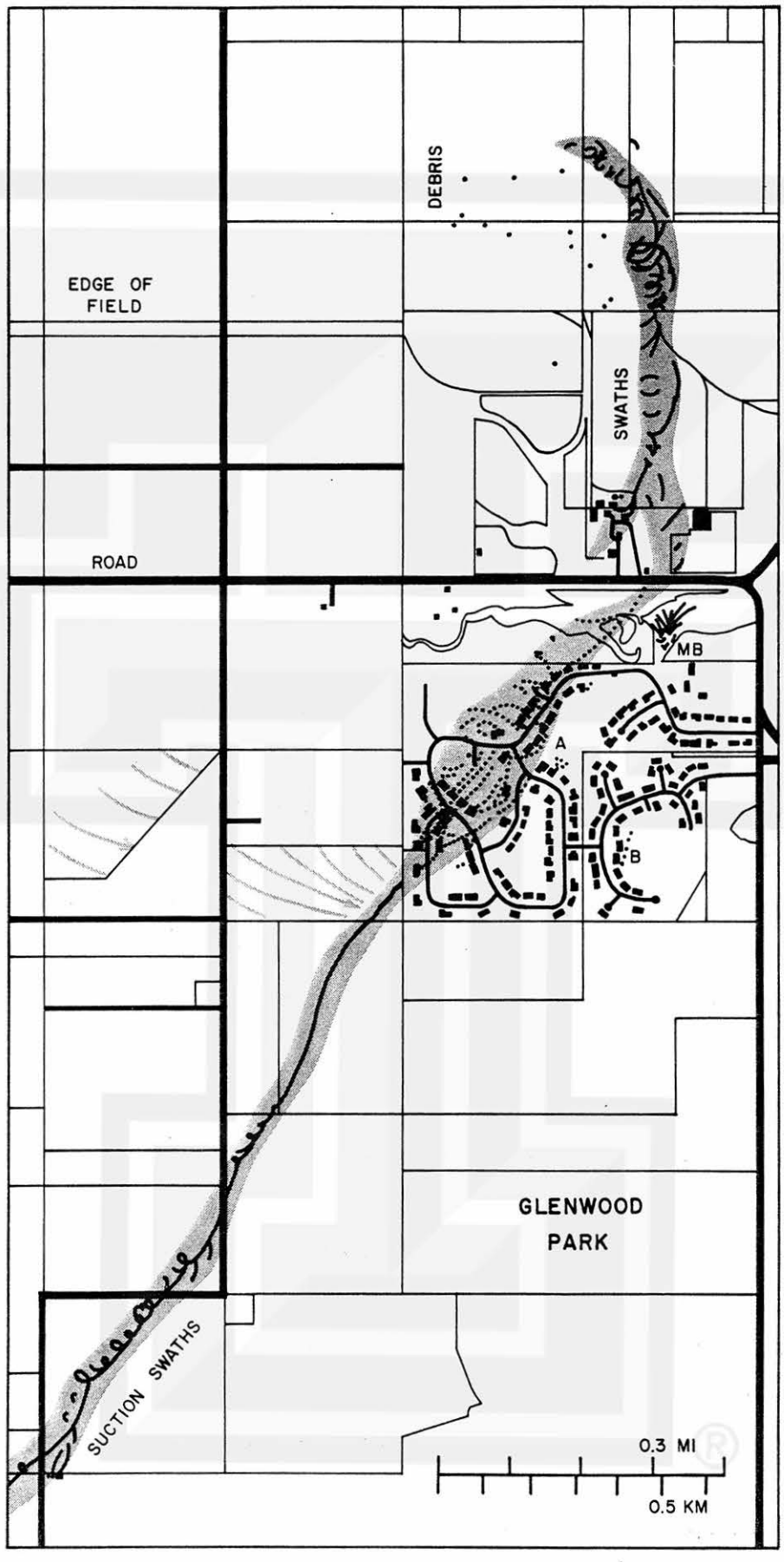

Figure 58. A portion of the path of the Glenwood Park tornado.

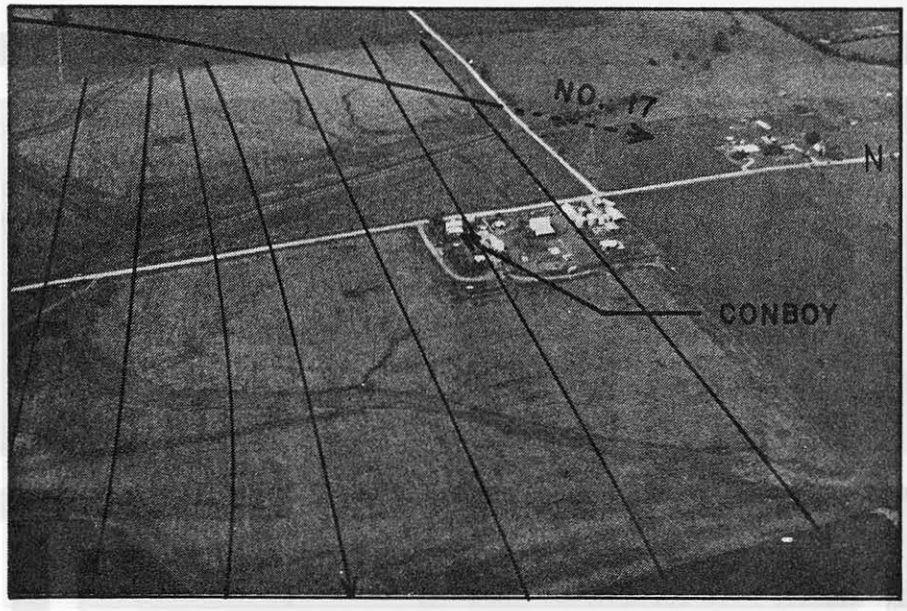

Figure 59. Relation between microburst damage and tornado damage (m 16 and tornado 17).

ACKNOWLEDGEMENTS

The authors are grateful for the eyewitness accounts given by scores of cooperative residents. The authors appreciate the discussions with Professor Ted Fujita who participated in the analysis (Fujita, 1978). The research was sponsored by the Nuclear Regulatory Commission under Contract No. 04-74-239, by the National Oceanic and Atmospheric Administration under Grant No. 04-4-158-1, and by the National Aeronautics and Space Administration under Grant No. NGR 14-001-008.

REFERENCES

Fujita, T. T. (1976): Spearhead echo and downburst near the approach end of a John F. Kennedy Airport runway. SMRP Res. Paper 137, The Univ. of Chicago, 51 pp. See also Fujita and Byers (1977).

Fujita, T. T. (1978): Manual of downburst identification for Project NIMROD. SMRP Res. Paper 156, The Univ. of Chicago, 104 pp.

Fujita, T. T. and H. R. Byers (1977): Spearhead echo and downburst in the crash of an airliner. Mon. Wea. Rev., 105, 129-146.

Fujita, T. T., G. S. Forbes and T. A. Umenhofer (1976): Close-up view of 20 March 1976 tornadoes: Sinking cloud tops to suction vortices. Weatherwise, 29, 116-131.

Idso, S. B. (1974): Tornado or dust devil: The enigma of desert whirlwinds. Amer. Sci., 62, 530-541.

Ryan, J. (1977): High wind, rain force two airplanes down. The State Journal-Register, Springfield, Illinois, August 7, 1977, pp 1-2.

Towery, N. G. and G. M. Morgan, Jr. (1977): Hailstripes. Bull. Amer. Meteor. Soc., 58, 588-591.